Stanev, E.V.; Pein, J.; Grashorn, S.; Zhang, Y.; Schrum, C.:
Dynamics of the Baltic Sea straits via numerical simulation of exchange flows.
In: Ocean Modelling. Vol. 131 (2018) 40 - 58.

First published online by Elsevier: 21.08.2018

https://dx.doi.org/10.1016/j.ocemod.2018.08.009

Dynamics of the Baltic Sea Straits via Numerical Simulation of Exchange Flows

E. V. Stanev[1], J. Pein[1], S. Grashorn[1], Y. Zhang[2], and C. Schrum[1]

[1]Institute of Coastal Research, Helmholtz-Zentrum Geesthacht, Max-Planck-Straße 1, D-21502 Geesthacht, Germany

[2]Virginia Institute of Marine Science, College of William & Mary,1375 Greate Road, Gloucester Point, VA 23062, USA

Highlights:

Two-layer exchange is adequately resolved with a resolution of ~100 m.

Horizontal resolution in the narrow channels has a large effect on the strait exchange.

Dynamics of strait exchange greatly differs in the individual straits.

Two-layer transport and blocking show non-unique dependence upon the net transport.

Large vertical mixing characterizes gravity currents in the Sound.

Abstract

The Semi-implicit Cross-scale Hydroscience Integrated System Model (SCHISM), which uses unstructured grids, is set up for the North and Baltic Seas. With a resolution of ~100 m in the narrow straits connecting the two basins, this model accurately resolves the inter-basin exchange. Validation against observations in the straits shows the model has good skill in simulating the transport and vertical profiles of temperature, salinity and currents. The timing and magnitude of the major inflow event in 2014-2015 is also realistically simulated. The analysis is focused on the two-layer exchange, its dependence on the atmospheric forcing, and dominant physical balances. The two-layer flows in the three connecting straits show different dependencies upon the net transport. The spatial variability of this dependence is also quite pronounced. The three-strait system developed specific dynamics, with time lags and differences between currents in the individual straits during inflow and outflow conditions. Analysis on the impact of resolution

indicates that the performance of the model changes depending on whether the narrow parts of the straits are resolved with a resolution of 500 m or 100 m. With this ultra-fine resolution, gravity flows and variability of salinity in deep layers is generally more adequately simulated. This paper identifies the needs for more profound analysis of the coupled dynamics of Baltic and North Seas with a focus on the Danish straits.

1. Introduction

European straits linking different semi-enclosed seas or connecting them with the ocean (e.g., the Bosporus, Dardanelles, Great Belt) are from one to several kilometers wide. The net transport in those straits is largely driven by river runoff. The shallow depths (~30 m at places) keep the hydrological characteristics of adjacent basins very different. A two-layer exchange, which is similar to the transport in tidal estuaries, dominates the straits' dynamics, with upper-layer transport to basins that are more saline and bottom-layer transport in the opposite direction.

The Danish Straits between the Baltic Sea and North Sea (Figs. 1, 2) include the Little Belt, Great Belt, and Øresund (commonly known in English as the Sound). The widths of the above straits are ~1km, ~15–32km, and ~4km, respectively. The comparison of these geometrical scales with the internal (baroclinic) Rossby radius of deformation (~5km in the Kattegat, see Fennel et al., 1991) indicates that the Great Belt could be rotationally influenced.

Tides are small in the Baltic Sea and most of the mechanical energy input is provided by air pressure and wind. The balance between the pressure gradient and friction roughly dominates flow regime in the straits. The analysis of cross-channel density structure by Umlauf and Arneborg (2009a, b) reveals dynamics that are more complex; the observed transverse Ekman transport is balanced by the geostrophic transport due to the down-channel tilt of the interface. In the Baltic Sea, there also are numerous sills critical to the separation between sub-basins and water exchange (Leppäranta and Myrberg, 2009). Thus the processes over the shallows are important for the internal mixing and transport of surface and bottom waters (Reissmann et al., 2009).

Much progress has been made in recent decades in the physical oceanography of the Baltic Sea (Feistel et al., 2008, Leppäranta and Myrberg, 2009), including a growing understanding of the role of Baltic Sea's straits and sills (Omstedt et al., 2014). One of the major gaps in our regional knowledge is in the field of exchange between sub-basins, turbulent mixing (Reissmann et al., 2009) and water mass formation. These processes are crucial for the deep-water ventilation (Meier et al., 2006) and upwelling in the Baltic Sea (Lehmann and Myrberg, 2008). So far, the

physical oceanography of the Baltic Sea is rather incomplete because in most modelling studies the two-layer exchange is neither sufficiently resolved nor considered as fully (two-way) coupled with the general circulation of interconnected basins. Elucidating and solving some problems in this field is the basic motivation for the present study and the main difference from our previous studies (Stanev et al., 2015; Zhang et al., 2016).

The water and salt balances, which are intimately related to their major physical drivers, such as evaporation, precipitation and river run-off, are at the heart of dynamics of estuarine basins. However, these balances are largely dependent on the dynamical control in the straits connecting the semi-enclosed basins and open ocean, and in particular on the atmospheric and tidal forcings. There are a number of process studies dealing with hydraulics in the straits, two-layer exchange and outflows, which captured the basic physics (Stigebrandt, 1983; Armi, 1986; Armi and Farmer, 1988; Farmer and Armi, 1988; Borenäs and Lundberg, 1986; Pratt and Lundberg, 1991; Laanearu and Lundberg, 2000; Gustafsson, 2004; Garrett, 2004; Arneborg, et al., 2007). There are also many 3D numerical model studies (Lehmann, 1995; Schrum, 1997; Schrum & Backhaus, 1999; Meier et al., 1999; Janssen, 2002), some of which show large bias in the water balance and a tendency towards reduced salinities. As recognized by Janssen (2001) and Omstedt et al. (2014), the ability of the models to simulate saltwater inflows through the Kattegat into the Baltic Proper, to continuously renew the Baltic deep water and keep the halocline stable is a prerequisite for multi-year simulations of the Baltic Sea.

In earlier 3D modelling studies, the transition zone between the Baltic Sea and North Sea (hereinafter the area including the Kattegat, Danish straits and the western part of the Baltic Sea will be referred to as the North Sea–Baltic Sea Transition Zone, NBTZ) was resolved in the best case with grids of ~1 km, and even coarser in scenario studies. This resolution is not optimal for narrow straits such as the Sound or Little Belt. Cross-sectional area in the straits depends also on the position of sea level, which is not fixed; therefore climate model scenarios (Meier et al., 2017) could be affected by sea-level rise. Sensitivity to global changes is expected to be strongest in the shallow straits where the dynamic balances could change if sea-level change is comparable with the depth.

Some positive trends of the structured-grid modelling of water exchange between the North Sea and Baltic Sea with respect to model resolution requirement are documented by Gräwe et al. (2014) who used a multi-nested modeling system with horizontal resolution ranging between 8 km and 600 m in the straits. Mohrholz et al. (2015) also reported model simulations with resolution of 600 m. Even with this fine resolution, models cannot fully resolve the geometry of the Little Belt, or the complex topographic structures of the other two straits. Therefore another strong motivation for this study is to investigate the model performance when using ultra-fine resolution scales, e.g., between 100 and 500 m.

Using one-way nesting techniques is also not adequate to address the dynamics of inter-connected basins (e.g. the coupled system North Sea – Baltic Sea). In this case, the possible interaction between dynamics in the straits and in the basins connected by the straits is missing. Thus insufficient model resolution and one-way nesting are considered the major sources of uncertainties and explain the limited or controversial knowledge of the straits' role in the dynamics of the European seas.

The key (and different) role of individual Baltic Sea straits and sills in water exchange and mixing still remains largely unclear. One problem revealed by the field campaigns is the intermittent regime of straits exchange and diverse appearances of inflow and associated mixing and entrainment, all of which have relatively small spatial scales. A clear 4D view based on observations on temporally variable inflows and outflows in the straits areas is still missing. Numerical modelling is considered here as an important research tool (as complementary to observations) to address the complexity of straits dynamics.

Unstructured-grid models overcome some nesting and resolution problems and allow addressing various ocean and coastal scales at the same time (Lermusiaux et al., 2013; Danilov, 2013; Scholz et al., 2013, Stanev et al., 2017). The simulation of water exchange in the NBTZ (Zhang et al., 2016a) also demonstrated promising perspectives. Earlier, Kliem et al. (2006) described simulation for the Baltic Sea using a 2D unstructured-grid model.

In the present study, we describe the improvements in the set-up used here in comparison to the model of Zhang et al. (2016a) for the same area. It is not possible in a single study to address all interesting physical aspects studied in several dozen previously published papers. Therefore we will focus our analysis on (1) model validation against observations in the NBTZ, (2) the role of resolution, (3) responses to atmospheric forcing with time scales ranging from synoptic to annual, and (4) the appearances of the two-layer strait exchange in the individual straits. Dynamics studied earlier will be presented in more general terms just to demonstrate the consistency of the present numerical simulations with the previous studies. This study is an extension of the work of Zhang et al. (2016a), but focused on the major Baltic Sea Inflow (MBI) in 2014-2015. It adds to the study of Stanev at al. (2015), which addressed simulations of earlier MBI-s and the inter-dependence between transports in the individual straits. One improvement here is that we increase the horizontal resolution in the straits by about ten times compared to the 0.5 nm horizontal resolution of Stanev et al. (2015), who used a two-way nested modelling approach. Another new aspect is the more profound model validation in the NBTZ and inter-comparison of results from numerical simulations using grids with different resolutions.

One specific research challenge (not addressed in our previous studies) motivating the present study is the impact of sea level dynamics on the variability of water and salt exchange in the North Sea and Baltic Sea. This issue is relevant to the causality of inflow events. We will also address the interdependency of the exchange flows in the individual straits and the temporal and spatial variability of the two-layer exchange. In a following publication the emphasis will be on the quantification of individual processes governing the two-layer exchange and mixing in the NBTZ.

153 The paper is structured as follows: Section 2 presents the numerical model; its validation against
154 observations is presented in Section 3; Sections 4 and 5 describe the circulation in the NBTZ and
155 its temporal and spatial variability; Section 6 addresses the response of individual straits to
156 atmospheric forcing and regional inter-dependence between straits transport and sea level;
157 Section 7 presents the two-layer exchange in the three straits connecting the North Sea and the
158 Baltic Sea; and, Section 8 quantifies the advantage of using ultra-fine resolution in the straits.
159 The paper ends with a brief conclusion.
160

161 **2. Numerical model**

162 **2.1 Model description**

163 Semi-implicit Cross-scale Hydroscience Integrated System Model (SCHISM) is a derivative
164 product of the original SELFE (semi-implicit Eulerian–Lagrangian finite-element) model (Zhang
165 and Baptista, 2008), with many improvements described in Zhang et al. (2016b). SCHISM
166 solves the primitive equations using a hybrid Finite Element and Finite Volume approach (an
167 example of the grid is shown in Fig. 3a). Terms that place stringent stability constraints (e.g.
168 CFL) are treated implicitly. Eulerian-Lagrangian method (ELM) is used for the momentum
169 advection. The model version used in this study is hydrostatic with Boussinesq approximation.
170

171 The combination of Galerkin Finite Element Method (GFEM) with (1) the implicit time-stepping
172 (which enables efficiency and robustness) and with (2) the ELM enables a good balance in terms
173 of numerical diffusion and dispersion, because numerical diffusion (inherent in an implicit
174 method and ELM) balances out by the numerical dispersion (inherent in GFEM). The model is
175 not immune to sensitivity with respect to grid generation (see next section).
176
177

178 SCHISM has been previously used to simulate the circulation in the North Sea and Baltic Sea
179 (Zhang et al., 2016a) and therefore its presentation here is very short. The parameterizations (see
180 Zhang et al., 2016a, b) allow resolving the baroclinic instability, which is very important for
181 areas dominated by eddy dynamics. Bottom roughness is set to a constant value of 0.5mm; the
182 bi-harmonic viscosity used is described by Zhang et al. (2016b). No explicit horizontal
183 diffusivity is used as the higher-order solver is monotone by design; the vertical viscosity and

184 diffusivity are calculated from the generic length-scale model (Umlauf and Burchard, 2003) with
185 a k-kl configuration. The improvements in the present paper compared to the setup of Zhang et
186 al. (2016a) are basically associated with better resolution in some critical areas and with
187 improved forcing.
188
189 **2.2 Model area**
190 Bathymetry data used in the present study are the same as the ones used by Zhang et al. (2016a).
191 However, additionally we use here the Baltic Sea Bathymetry Database version 0.9.3
192 (http://data.bshc.pro/, last accessed on June 5, 2015) with 500 m resolution to improve the
193 bathymetry in the NBTZ. Model refinements (compared to bathymetry and grid of Zhang et al.,
194 2016a) have also been done in Skagerrak, Norwegian Trench, Wadden Sea and the area around
195 the mouth of Oder River.
196
197 The computational grid has ~400K nodes (compared with about 300K nodes in the topography
198 of Zhang et al., 2016a) with a minimum grid side length of ~80m in the narrow areas of the Little
199 Belt (Fig. 3). The model grid for the other two straits is shown for example in the supplementary
200 material (Fig. S1 and Fig. S2). Most of the change of resolution is specified on the shallow shelf
201 where dynamics are dominated by friction. An essentially uniform resolution of ~3 km is used in
202 the open-sea parts of two basins minimizing wave distortion because of non-uniform resolution
203 in unstructured grid models. The vertical LSC^2 grid described by Zhang et al. (2015) is used here
204 (see Fig. 3b). It allows flexible placement of vertical nodes at each horizontal position; the
205 Vanishing Quasi Sigma (VQS, Dukhovskoy et al., 2009) ensures smoothness among neighboring
206 nodes. Shaved cell technique (Zhang et al., 2015) eliminates staircases, shuts down the diapycnal
207 mixing and reduces the co-ordinate slope and thus the pressure gradient errors. Tests conducted
208 to demonstrate the performance of the LSC^2 grid can be found in Zhang et al. (2015). As
209 demonstrated by Zhang et al. (2016a) on the example of Baltic proper (see their figure Fig.A.1**)**,
210 the use of LSC^2 grid contributes to simulating realistic stratification. This couldn't be achieved in
211 *S*-grid even with the number of layers being doubled. The vertical LSC^2 grid used here consists
212 of up to 59 layers in the Norwegian Trench, with an average number of 31 levels in the whole
213 model domain.
214

2.3 Initialization and forcing

Monthly climatological salinity and temperature data (Janssen et al., 1999) are used to initialize the model, like this was the case in the paper by Zhang et al. (2016a). However, we use here finer-resolution data for atmospheric forcing, including hourly wind, atmospheric pressure, air temperature, dew point temperature and cloud cover from the 7 km-resolution COSMO-EU model of German Weather Service (DWD). From these data, the wind stress, fluxes of sensible and latent heat, as well as short wave and long wave radiation are computed. The Swedish Meteorological and Hydrological Institute (SMHI) EHYPE (pan-European HYdrological Predictions for the Environment) product is used for the freshwater fluxes from 34 rivers discharging into the Baltic Sea and North Sea.

The model has two open boundaries (west of the English Channel and between the British Isles and Scandinavia, Fig. 1). At these boundaries hourly values of elevation, horizontal velocity, salinity, and temperature were used, which were taken from the Copernicus product (http://marine.copernicus.eu/; last accessed in May 2017) interpolated at each time step onto the model grid. The use of these data is considered an optimal solution because they are dynamically consistent, based on up-to-date modelling (O'Dea, 2012) and have been validated extensively.

After an initialization period of four years the model is run for another two years, 1 March 2014 to 31 March 2016, which is the period analyzed in this paper. We will refer to this reference experiment as the control run (CR). An additional experiment was carried out in which all areas in the NBTZ where the resolution in the CR was finer than 500 m were resolved with a horizontal resolution of 500 m. We will refer to this experiment as the E-500. Comparison between Fig. 3c, d and Fig. 3a, b illustrates the difference in the model resolution of two experiments for the area of Little Belt. Fig. S1 and Fig. S2 illustrate the difference between the CR and E-500 for the straits of Sound and Great Belt, respectively.

The simulations were conducted on Mistral peta-scale supercomputer of the German Climate Computing Center (Deutsches Klimarechenzentrum GmbH (DKRZ)). On 1024 CPUs the model runs ~150 times faster than real time.

3. Validation against observations

3.1 Sea level and transport in the straits

The overall performance of SCHISM for the area in the present study has been addressed by Zhang et al. (2016a). Therefore the validation here will focus primarily on areas and specific periods, which have not been addressed in this earlier study, and include the NBTZ and periods of recent extreme events. The studied period is chosen such that it includes the MBI in 2014-2015, for which there are already observations (Mohrholz et al., 2015) and analyses. The realism of the model with respect to the transport in the straits will be assessed. We will compare our estimates with the computations based on the method proposed by Håkansson (citation from Meier et al., 2003), which assumes a balance between along-strait pressure gradient and bottom friction term. This dominant balance is proven in those studies after estimating the correlation between sea level difference in two locations at both sides of the straits and the observed volumetric flows obtained from ADCP ship-borne transects and moored Aanderaa current meters across the Drogden Sill. The calibration proposed by those authors used the two tide gauge stations Viken and Klagshamn, located in the northern and southern entrance of the Sound, respectively (see Fig. 2 for their positions).

The index of agreement *D* proposed by Willmott (1981) measures the degree to which the observed data *O* is estimated by the predicted value *P*,

$$D = 1 - \frac{\sum_{i=1}^{n} (P_i - O_i)^2}{\sum_{i=1}^{n} (|P_i - \bar{O}| + |O_i - \bar{O}|)^2}. \quad (1)$$

Here, *n* is the number of observations (index *i)* and the overbar is the temporal mean of the observed data. A value of 1 would indicate perfect agreement, whereas a value of 0 would indicate no agreement at all. In the third and fourth line of Table 1, P and O are the normalized transports estimated from the parametric model presented by Meier et al. (2003) and numerical model, respectively.

The observed and simulated sea levels at these two stations are in a very good agreement (Fig. 4a-b and Table 1). Noteworthy is the phase difference between sea level at these stations (compare Fig. 4a and Fig. 4b). The pressure gradient between the two of them changes to strongly negative (Fig. 4e) giving the first “push” of the MBI in 2014. The timing of this event is

shown by the vertical green line. The model errors are small in comparison to the variances of analyzed variables and therefore *D* is quite high. The index of agreement from the parametric model of 0.97 is considered here as an "ideal" agreement because it is based on calibrated data. Our simulations yield 0.94, which demonstrated that the agreement between the observations and the fluxes (Q_m) computed with SCHISM is very close to that "ideal" case.

	D	**RMSE**	**B**
ξ_obs, ξ_m (Viken)	0.88	0.15 (m)	0.04 (m)
ξ_obs, ξ_m (Klagshamn)	0.92	0.09 (m)	0.10 (m)
Δξ_obs, Q_par (normalized)	0.97	0.33	-0.03
Δξ_obs, Q_m (normalized)	0.94	0.42	-0.08

Table 1. Index of agreement, root mean square error (rmse) and bias of sea levels (first and second lines) at the gauges Viken and Klagshamn (see Fig. 2 for their positions). The agreement between the normalized (non-dimensional) data series of sea-level differences between the same stations and the net transport estimated from the parametric model of Håkansson (citation from Meier et al., 2003) are shown in the third line. The present simulations are shown in the fourth line.

The temporal evolution of sea level (Fig. 4a, c) up to the Baltic Sea stations Visby and Degerby, the latter known recently as Föglö, (see Fig. 1 for their position) demonstrates a synchronous sea-level dynamics over a larger area (the green vertical line shows that phase differences are relatively small). These stations are representative of the volume change of the whole Baltic Sea (e.g. Jacobsen 1980). As demonstrated by Janssen et al. (2001), Station Degerby has high skill in describing the variability of Baltic Sea surface elevation. The accurate predictions of sea level elevation in stations Visby and Degerby manifests the model skill with respect to the dominant dynamics in the Baltic Sea.

According to Håkansson (citation from Meier at al., 2003), the agreement between the observed and simulated sea levels at stations Viken and Klagshamn guarantees a correct prediction of the

volumetric transport through the Sound. This concept is based on the assumption of balance between along-strait pressure gradient and bottom friction term. It is supported by the third and fourth lines in Table 1, which show the agreement between non-dimensional sea-level differences at these two stations and net transport (see also Fig. 4e). Notably, the parametric estimations of Håkansson were calibrated to observations; SCHISM was not specifically calibrated. These results indicate that also in SCHISM the balance between along-strait pressure gradient and bottom friction plays the major role in the Sound. Furthermore, the correct estimate of the straits' transport is a prerequisite for the good model skill in the entire Baltic Sea. Obviously, the good skill in stations Visby and Degerby (Fig. 4a, c) and in the straits are consistent with each other.

3.2 Currents in the straits

Data from three ADCP stations in the Danish straits operated by the DMI are used here to validate simulated currents. Two stations, Østerrenden (55.363266N 11.022787E) and Vengeancegrund (55.207542 N11.086632E), are in the Great Belt, and the third , Drogden Fyr (55.536380N 12.711413E), is in the Sound (see Fig. 2 for their position). Data used here are recorded at 3 depths at all three stations during 01 October 2014-01 June 2015. Comparison with simulations demonstrated a good qualitative agreement at the three stations (Fig. 5). The model overestimates slightly the velocity maxima. The quantitative validation shows that the coefficient of agreement is above 0.82, reaching 0.94 at Vengeancegrund (Table 2). Compared to the relatively large amplitudes of currents the rms error is not too big. The maximum bias is ~6 cm/s, which is also reasonable, keeping in mind that model forcing is not perfect.

Station, depth	**D**	**RMSE [m/s]**	**B [m/s]**
Drogden, 3m	0,86	0,39	-0,010
Drogden 5m	0,93	0,29	-0,010
Drogden 10m	0,91	0,18	-0,041

Vengeancegrund, 1m	0,94	0,28	-0,028
Vengeancegrund, 3m	0,93	0,30	-0,033
Vengeancegrund, 5m	0,94	0,28	-0,048
Oesterende 5m	0,86	0,38	0,042
Oesterende 10m	0,87	0,34	0,054
Oesterende, 14 m	0,82	0,29	0.064

Table 2. Index of agreement (D), rmse and bias (B) of observed along-channel currents and currents estimated by the model (see Fig. 2 for the positions of observations).

It is noteworthy that the signals in the two straits differ substantially not only by their magnitude, but also by phase.

3.3 Salinity

Earlier validations of SCHISM against MARNET observations (http://www.bsh.de/en/Marine_data/Observations/MARNET_monitoring_network/index.jsp, last accessed July, 2017) revealed a good consistency of simulations (Zhang et al., 2016a). In the following, we will present model validation against different data source, e.g., freely available CTD and bottle data from the International Council for the Exploration of the Sea (ICES) database (http://ocean.ices.dk/HydChem/HydChem.aspx?plot=yes, last accessed July, 2017). From this dataset we selected the observations situated along the pathway of salt intrusions (BY-1, BY-5, BY-7 and BY-15; see Fig. 1 for their positions). The validation was performed for a period of one year starting 1 September 2014 and thus covering the time of the MBI during the winter 2014-2015.

The ability of model to capture the change of thermohaline characteristics of the North Sea waters penetrating into the Baltic Sea during the MBI along their way over the sills and in the

small regional sub-basins is illustrated in Fig. 6. Simulations and observations show clearly the delayed appearance of salt-water intrusions with increasing distance from the straits, as well as a decrease of the amplitude of salinity outbreak associated with the MBI at stations far from the NBTZ. The model skill is good (D is above 0.91 in bottom layers in all stations). In the surface layers D is also above 0.91. Only in stations BY-7 and BY-5, D drops to 0.80 which is a reasonable value taking into consideration possible errors in the model and its forcing. Namely, using hourly data with 7 km horizontal resolution is perhaps still not fine enough. Since the Baltic Sea is enclosed basin, unresolved atmospheric dynamics in its large coastal areas could bias ocean simulations. Bulk aerodynamic formulas are also not perfect. Using coupled atmosphere-ocean models with high resolution in the straits and other sensitive areas could be an adequate step toward improvement of atmospheric forcing.

The time versus depth diagrams of salinity (Fig. 7) demonstrate that the time when the mixed North Sea water reaches the observational locations is very well forecasted by the model. In the stations Darss and Arkona simulated salinity values exceed the observed ones, while in the Gotland Basin simulated bottom salinity values are slightly underestimated (compare Fig. 7g and Fig. 7h). Although peaks in salinity associated with the MBI are slightly overestimated in the shallow NBTZ area, the mixing on their way down to the Gotland Basin reduces the magnitude of salinity signal below the observed values. The agreement between simulations and observations in the Gotland Basin is very valuable because the Gotland Basin integrates temporal development of salinity in the Kattegat, Belt Sea and the Western Baltic (Janssen et al., 2001). In conclusion, without special tuning, the model captures salinity intrusions in the straits. The deterioration of the bottom water properties in E-500 will be addressed in section 8 (see the panels on the right of Fig.7). More realistic representation of the penetration of mixed water down to the Gotland Basin and its spreading there could be achieved after a closer look at the parameterizations used, which will be addressed in future publications

4. Overall presentation of the circulation in the NBTZ.

The model allows resolving sharp fronts in salinity (the panels on the left-hand side of Fig. 8) and numerous small-scale features in the relative vorticity (the panels on the right-hand side of Fig. 8). The comparison between the inflow and outflow patterns demonstrates that the position

of positive and negative vorticity alternates; that is demonstrated well in the Great Belt. The vorticity alternation follows the alternating direction of flow in the straits. With a much coarser resolution, as used in earlier modelling studies based on structured grids, one cannot accurately resolve the velocity gradients in the straits. The zoom-in views of the model grid in Fig. 3 (see also supplementary Fig. S1_and Fig. S2) and the insets in the Sound and Great Belt shown in Fig. S3 support this conclusion. The complex flow structure could be important for the resistance in the straits, which depends on the velocity shear. The above reasoning is supported by the analysis on the role of horizontal resolution (CR versus E-500) presented in section 8. With increasing distance from the straits, the scales of vorticity patterns increase. Most of them show an elongated shape, which is explained by the predominant narrow jets in the area of the Arkona and Bornholm Basins.

The inflow and outflow situations are well distinguished in the salinity patterns (Figs. 8a, 8c). During the outflow conditions low salinity surface water displaces to the north (see also the sharp front in Fig. S3e, f), resulting in a reduction of sea surface salinity (SSS) in the Kattegat by about 6. The propagation pathways of these low-salinity water masses are well seen in the plumes originating from the Great Belt and Sound (Fig. 8a). The salinity front separating the Skagerrak water mass from the Kattegat water mass is “pushed” north of the Skagen (Fig. 8a). In most inflow cases, the Skagerrak water (with higher salinity) depicts a jet-like propagation pattern in the direction of the Sound. The front separating these two water masses is extremely strong, reaching more than 10 salinity units per km (Fig. S3f) at certain times. The two straits provide two sources of high salinity water entering the Bornholm Basin (Fig. 8c).

The vertical salinity section through the Sound shows a typical gravity-current type propagation starting from the Drogden Sill (the shallowest location in Fig. 9). This current is seen even better in the turbulent kinetic energy (TKE) patterns; maximum values are in a thin bottom layer. TKE shows another maximum zone at the northern entrance of the Sound where the jet from the Kattegat converges towards the strait (Fig. 8c). This is a zone of extreme vertical mixing; its dynamics can change vertical stratification and strongly affect the propagation properties of gravity currents.

The TKE decreases in the middle of the water column, particularly in the Baltic Sea part of the cross-section. It further increases in the surface layer, displaying a characteristic profile known from other similar strait environments (Stanev et al., 2017).

5. Temporal and spatial patterns of inflows and outflows.

5.1 Chronology of the MBI in 2014-2015

Inflows and outflows in the Danish straits have much in common with tidally driven estuarine exchange; however in the case of the Baltic Sea the role of atmospheric forcing is more important than that of tides (Stanev et al., 2015). MBIs are to a first order barotropic phenomena driven by an emptying-refilling process of the Baltic Sea (Schimanke et al., 2014). Existing concepts explaining their chronology have been mostly based on observations (Lass and Matthäus, 1996). However, observations are not available over large areas and for sufficiently long periods. Furthermore, MBIs appear rarely (about once per ten years in the recent times) and their statistical description is difficult. Numerical modelling provides an opportunity to address the timing and causality of MBI for the entire area of inter-connected basins.

The temporal-spatial evolution of MBI during 2014-2015 is presented in Fig. 10 along the section line shown in Fig. 1. In the area of the straits this line follows the section line through the Sound as shown in Fig. 2. Sea level in the Baltic Sea is higher than in the North Sea; this is typical in estuarine basins. The mean difference between the areas to the left and to the right of Drogden Sill (see the blue arrows in Fig. 10) is ~17 cm. This sill (the shallowest depth in Fig. 9) physically separates the two basins as seen by the variability pattern in Fig. 10a (we will come again to the “separation issue” in section 6.1). In the North Sea, the temporal variability is dominated by tides. For better readability of plots, model data have been filtered with a window of 1 day, so only neap-spring variability is seen in Fig. 10.

Sea level variability in the Baltic Sea is largely driven by atmospheric forcing; the event at the beginning of December 2014 is of particular importance. On 2 December 2014 (triangle symbol on the time-axis in Fig. 10a), sea level in the Baltic Sea dropped to ~52 cm below the sea level found to the north of the Sound (see also Fig 4 manifesting the precursory period). In only 2 days this slope triggered a huge transport (MBI) resulting in an increase of sea level in the Baltic Sea

by 82 cm during the next ~40 days (Fig. 4c, d). A similar situation was observed in November 2015, this time the MBI appearing as two strong pulses in the winter of 2015-2016 (Fig. 10a).

The presentation in Fig. 10a is instructive also for some important general circulation features. One feature is the low sea level at km 800 (in the Skagerrak) that reflects the cyclonic rotation of currents there. As seen in Fig. 10e, bottom salinity in the Baltic Sea shows an increase (positive anomaly) right after the outbreak of MBI in 2014. This signal propagates to the east, which is deduced from the slope of the salinity anomaly pattern. The speed of propagation decreases with increasing distance from the strait, particularly approaching the Gotland Basin. This basin is the "final destination" of positive bottom salinity anomaly (compare with the delay of phases of salinity signal illustrated by the blue line in Fig. 6). There is not a clear response of the bottom salinity in the North Sea to the MBI, which is easily understandable. However, this does not hold for the SSS. Indeed the surface plume propagation depicts situations with alternating positive and negative anomalies, which propagate to the west (the slope of contours in the North Sea, Fig. 10c is opposite to the one in the Baltic Sea, Fig. 10e). The overall temporal variability is approximately seasonal. What seems non-trivial is that the largest positive anomalies on both sides of the Drogden Sill are generated almost simultaneously and propagate in both directions as surface plumes in the North Sea and bottom plumes in the Baltic Sea. Another interesting result of the simulations is the entrapment of saltier water at about km 1500, which is the area of Bornholm Basin (red arrows in Fig. 10). This basin accumulates saltier water and acts as a long-term reservoir, which sporadically "discharges" parcels of salty water to the east. This is seen as short-term positive-anomaly "strips" following the direction of bottom water propagation. While the presence of these strips is consistent with the dominant concept about the periodic export of saltier bottom waters from the retention basins (e.g., the Bornholm Basin, Jakobsen, 1995), an explanation of the "vertical strips" seen in the bottom salinity anomaly is needed. This is not an unphysical result. Its appearance is explained by the fact that the anomalies of bottom salinity depend on the position of the chosen thalweg, as well as on the vertical stratification; the latter is highly variable in different depth intervals.

5.2 Different dynamics in the three straits

Comparison of the SCHISM simulations in the three straits (Little Belt, Great Belt and Sound) are shown in Fig. 11. In order to give more detailed views on the results, time versus distance diagrams in these figures are shown only in the NBTZ, that is along the section lines in Fig. 2. While the pressure gradient forcing appears in a semi-coherent way in the three straits, the temporal-spatial response of individual straits to atmospheric forcing is rather different. The sea-level anomalies (left panels in Fig. 11a) are extremely large in the winter months of 2014 and 2015 providing the major drivers for the strong inter-basin exchange. This barotropic forcing triggers a clear salinity response in the three straits, which largely differs between the surface and bottom layers. In the Sound (Fig. 11b) pulses of higher-salinity surface water are very weak (and with a very small along-strait extension). However, bottom salinity pulses appear quasi-periodically in this strait (Fig. 11c); the strongest of them extends up to the Bornholm Basin (~km 300). The low-salinity values in the Sound area between km 150 and 250 in Fig. 11c do not mean an absence of salinity intrusions there, but demonstrate that these are shallow areas with salinity values close to the surface ones.

Saltier mixed North Sea water shows much longer excursions in the Great Belt, both in the surface and bottom layers, than in the surface layers of Sound. Great Belt section reveals the zones of saltier bottom waters in the Arkona Basin (about km 300). Note that the position of 300 km along the Sound pathway almost coincides with the position of 500 km along the Great Belt section (Fig. 2). These positions demarcate the Bornholm Basin, an area of salt-water accumulation. In the two straits, MBI is better identified by the salinity change in the bottom layers. The comparison between the sections along the Great Belt and Sound, which slightly overlap at the end of the Great Belt section, demonstrates that the high bottom salinity reflects the water originating from the Sound. This conclusion is justified by the fact that the bottom salinity maximum at about km 500 along the Great Belt section is separated from the main pulse of saltier bottom water.

The Little Belt shows more “diffuse” patterns, which is due to the fact that the narrow opening in this strait needs more time to propagate the saltier North Sea water. While the importance of the Little Belt for the exchange between the North Sea and Baltic Sea is small under normal events,

it becomes more substantial during the MBI. In the southernmost part of the section line in this strait (at about km 200) a backward propagation of positive salinity anomaly occurs, which is identified by the opposite slope of the contours in the time versus distance diagram. This illustrates the fact that saltier water in the Great Belt, which tends to fill the western Baltic Sea, reaches this location faster and in bigger amounts than water originating from the Little Belt.

6. Synchronous and asynchronous responses in the individual straits

6.1 Interdependence of straits transport and sea level

It is still unclear whether the changes of sea level in the Baltic Sea and North Sea are equally important for the net transport, and what the expected dependence during inflow and outflow situations is. To answer these questions we analyze first the dependence of the volume fluxes integrated over the threes straits on the difference between sea level in the Kattegat and central Baltic Sea. Unlike the analysis presented in section 3.1, which was focused on the dominant frictional control in the straits, the difference between sea levels in the Kattegat and central Baltic Sea reflects the role of general oceanographic conditions in the two basins and can potentially elucidate the leading role of one of them (see the discussion in section 3.1 about the representativeness of sea level in the central Baltic Sea).

The scatter plots in Fig. 12 are shown for two 14-days periods during which the transport was dominated by either outflow from the Baltic Sea (1-15 Nov, 2014) or inflow (6-21 Dec, 2014). As expected, there is a clear correlation between sea-level difference and net flow. The smaller correlation during the inflow situation (the period of MBI) is not so trivial and is explained with the help of Fig. 12d. The inflow period-1 was characterized by multiple pulses, which is consistent with a similar situation during the 1993 MBI (Stanev et al., 2015). This is comparable with the salinity change described by Jakobsen (1995): inflows were characterized by larger oscillations, while outflows showed smoother changes. Obviously, the 1993 case observed by Jakobsen (1995) was almost repeated in 2014-2015. The unstable dynamics during inflows thus makes it possible that large outflows occur in times of small sea-level differences between the Kattegat and Central Baltic Sea, i.e., oscillations of sea levels in the two basins and the strait flow could become asynchronous.

The correlation between the sea level differences betweenthe two basins and the sea level in the Kattegat (Fig. 12b), from one side, and the central Baltic Sea (Fig. 12c), from the other, demonstrates that the variability of sea level in the Kattegat plays the leading role (correlation ~0.91). Sea level in the central Baltic Sea correlates weakly with the sea level difference during outflows (correlation ~-0.38). Changes of sea level in the central Baltic Sea are more important for the inflows. In this case the correlation reverses with -0.73 and 0.5 for the Baltic Sea and the Kattegat, respectively. This result is reminiscent of similar results for the Black Sea-Mediterranean Sea system based on analysis of observations (Volkov et al., 2016) and numerical simulations (Stanev et al., 2017), i.e. the major driver is the forcing from the outside basin. However, inflows are strongly dependent on the sea level in the central Baltic Sea, which supports the existing concepts (Lass and Matthäus, 1996).

The areal distribution of correlation between net straits transport and sea level (Fig. 12e) reveals an overall anti-symmetric pattern (positive correlation in the Kattegat and negative correlation in the Southern Baltic Sea). With increasing distance from the straits, the magnitude of correlation decreases. This reflects the delay associated with the propagation of barotropic signal to remote locations. The areas of transition from positive to negative values are very sharp and identify the natural (physical) boundaries between the North Sea and Baltic Sea. The trend of larger negative correlations along the Scandinavian Baltic Sea coast reveals the role of geostrophic control. The larger correlation along the western coast of Kattegat is explained with the larger tidal range there (see Fig. 6 of Stanev et al., 2015).

6.2 Similarities and differences in the response of individual straits to atmospheric forcing.

Using a numerical model with horizontal resolution of 0.5 nm, Stanev et al. (2015) demonstrated that the correlation between transports in the Sound and Great Belt cannot be represented with a simple linear regression line. This does not fully conform to the simple idea that the transports in the straits are linearly proportional, the coefficient being the ratio between cross-sectional areas. There are different estimates for this ratio. Mattsson (1996) claims that the narrow passages in the Belt Sea have vertical cross-sectional areas on the order of 300 000 m^2, while the narrow cross-sectional areas in the Sound are about 60 000 m^2. They found that the mean partition of the instantaneous flows through the Great Belt Sea and Sound is 8:2, rather than the generally

563 accepted (at that time) estimate of 8:3. Kullenberg and Jacobsen (2000) reported a quite different
564 ratio between cross-sectional areas of two straits. They claimed that the cross-sectional area over
565 the sill in the Sound was 0.1 km^2; in the Belt Sea the narrowest section was 0.16 km^2. The ratio
566 between the transports in the two straits estimated by Sayin and Krauss (1996) was 3:1.The
567 estimations of Fischer and Matthäus (1996) and Jakobsen and Trebuchet (2000) for the transport
568 ratio (TR) was 2.67. The estimation of Fu (2013) was 2.78. Besides the ratio between transports
569 in the two strait, the response times are also subject to large uncertainties (Stanev et al., 2015).
570
571 One could expect that the differences between previous estimates of exchange flows were most
572 probably due to the use of different cross-sectional areas (more generally topographies). The
573 areas of narrowest cross-sections in the two straits based on the topography and model resolution
574 used in the present study are 121100 m^2 and 73000 m^2. The ratio between the smallest cross-
575 sectional areas of the Great Belt (between Nakskov and Langeland) and Sound in our model is
576 1.66. We will call this number area ratio (AR).
577
578 The barotropic transports in the Great Belt and Sound for October 2014- May 2015 indicate that
579 the magnitudes of oscillations in the two straits largely exceed the mean values (Fig. 13a). In the
580 Great Belt the the rms difference of barotropic transport from its mean value is 6.64 x 10^4 m^3/s;
581 the corresponding number for the Sound is 2.89 x 10^4 m^3/s, while the net transport for the Baltic
582 Sea is about 1.5 x 10^4 m^3/s (Liljebladh and Stigebrandt, 1996). The averaged TR for October
583 2014 - May 2015 estimated here is 2.70 (see the regression curve in Fig. 13b), which compares
584 well with the numbers 2.63-2.75 of Stanev et al. (2015) who used a model of the same area with
585 a resolution of 1 km. This result can serve as a justification that the TR is reasonably simulated
586 even with this “coarse” resolution of ~1km.
587
588 There is a substantial difference between the TR estimated from the regression curve (2.70) and
589 the AR (1.66) demonstrating that the narrower and shallower strait (Sound) exerts larger
590 resistance. The scatter plot (Fig. 13b) gives an idea about the robustness and stability of the
591 above averaged estimates. The comparison between this averaged number (2.70) and the large
592 variance of TR (2.30) demonstrated the complex inter-relationship between transports in the two

straits (see Fig. 13g) and their large variations over time. Stronger variability in the Great Belt compared to the Sound is partially due to high frequency (tidal) oscillations in the former; the Sound effectively filters out the tidal oscillations (Stanev et al., 2015).

The distribution of the TR is non-Gaussian (Fig. 13e). There is a clear inflow-tail, i.e. the transport in the Sound gets relatively stronger during inflow events. This tendency during inflows is illustrated in the comparison between Fig. 13c and Fig. 13d where the distribution of the TR is separately shown for inflow and outflow cases. Although the shapes of these histograms are not fully identical with the results of Stanev et al. (2015, compare with their Fig. 8) the overall result suggests that the change in transport starts first in the Sound. The temporal evolution of the distribution of the transport ratio (Fig. 13g) clearly explains the non-Gaussian shape of histograms.

The asynchronous responses of the two straits revealed by the asymmetry of the curve in Fig. 13f against zero time lag is explained as a result of the Sound being closer to the inflowing waters, which follow the eastern Kattegat coast (see Fig. 8c). Unlike the similar analysis in Stanev et al. (2015), we did not filter out the tides, therefore the lagged-time-correlation in Fig. 13f is affected by M2 tides.

The basic difference between the correlation of barotropic transports in the Little Belt and Great Belt (not shown here) from the case addressed above (Sound and Great Belt) is that the coefficient in the regression curve is about two times smaller, because the transport in the Little Belt is about half of that in the Sound. Notably, the average TR (5.11) is much smaller than its variance of 12.96 due to a very low correlation between the flows in the Little Belt and Great Belt.

7. Two-layer exchange in the straits

In some straits connecting estuarine basins with the neighboring seas, the net transport in the upper and bottom layers shows opposite trends. With the increase of net outflow, i.e. the transport in the direction of the long-term mean (barotropic) transport, the upper layer flow increases and the bottom flow decreases and is sometimes blocked. During the inflow situation,

the upper-layer transport decreases and the bottom layer transport increases (Möller, 1928). This old concept usually assumes that there are two water masses in the upper and bottom layers moving in opposite directions separated by an interface where velocity tends to zero. This is a typical situation in estuarine circulation. One such case is the Strait of Bosporus where the two-layer exchange is well known.

In the NBTZ the frontal area separating the Kattegat and Baltic Sea water masses is periodically displaced back and forth by the atmospheric forcing (Fig. 9a, c); the vertical structure of the two-layer flow is not always well pronounced, unlike in the Bosporus Strait (see for more detail Stanev et al., 2017) . The latter resembles a salt wedge where the interface is almost horizontal (slope of 1-2 m per kilometer) and covers the entire strait. The simulated dynamics in the Baltic Sea straits show rather different and more diverse appearances.

The lack of profile observations over large areas in the straits makes it impossible to validate extensively the two-layer volume exchange. We can at least compare the present simulations against other similar cases and check whether concepts valid for other straits hold for the Baltic Sea straits, whether this is the case everywhere in these straits, and what the differences are.

As shown in section 3.1 the volumetric transport is simulated reasonably well (Fig. 4). This (barotropic) transport integrated over the sections shown in Fig. 14a is used as the independent variable (x-axis in Fig. 14), against which we compare the transports in the upper and bottom layers across the same sections (y-axis). Along most of these sections, the simulated upper-layer flow decreases and the bottom-layer flow increases with decreasing net transport. This supports the previous estimates based on simulations with the same model and observations in other similar straits (Stanev, 2017). It is noteworthy that the model has not been specially tuned to earlier theoretical analyses, some of which were based on simpler theoretical concepts or observations. This demonstrates that these results have general applicability. What has not been sufficiently addressed in earlier analyses in the NBTZ is the spatial variability of the dependence of transport in each layer on the total net transport. This is illustrated in Fig. 14 for three sections in the Little Belt (on the left), four sections in the Belt Sea (in the middle), and four sections in the Sound (on the right). The positions of the analyzed sections are shown in Fig. 14a. The plots

on the top correspond to the northernmost transect, and the plot on the bottom to the southernmost transect.

The comparison between two-layer flows in the three straits shows similar trends, but the magnitudes are different (notice different ranges for each strait). With the exception of the northernmost section in the Sound (Fig. 14c) and the southernmost section in the Little Belt (Fig, 14j), all other plots show that in most cases the flow is unidirectional for most of the transport variability ranges. This means that either the surface or bottom flow equals the net transport, i.e. we observe a blocking of transport in one of the layers (Oğuz et al., 1990). As the magnitude of net transport decreases below some critical value the transport becomes two-directional; this transition is not linear as seen by the curvature of transport dependence.
In an idealized case, the surface and bottom transports can be represented by two crossing curves (Oğuz et al., 1990). This would mean that for one value of net transport there is one and only one pair of values for the upper and bottom layer transports. The scatter of data suggests that the appearance of two-layer transport is quite diverse (different possible combinations of surface and bottom flows could correspond to the same net transport). Furthermore, the scatter is different in different straits and at different locations in the straits. This manifests that there are not a unique critical values of net water transport, beyond which two-layer transport transforms into one-layer transport. Several representative examples are addressed below, one for each strait.

Extreme transports in the Little Belt are more than five times smaller than the extreme transports in the Great Belt. Two-way transport is observed for only very low net transports (below $3x10^3$ $m^3\ s^{-1}$=0.003 Sv). At the southernmost end of this strait the spread of data is large, which suggests that the two-layer transport there is substantially affected by other processes (e.g., the local circulation) after the flow leaves this narrow strait.

Along the entire Great Belt, from the northernmost reaches down to the Fehmarn Belt the transport curves look very similar. The largest scatter of data at the Fehmarn Belt and at the northernmost section is due to larger-scale oceanographic conditions that is in these areas simple concept of straits transport are not applicable. Blocking events for surface and bottom flows occur at different net transports, which is most pronounced for the section across Langeland

Fjord (Fig. 14h). In this case, the asymmetry of curves (left and right of the zero transport value) is clearly seen. Furthermore, for all sections there is no unique magnitude of net transport beyond which blocking events occur. At the Great Belt South section (Fig. 14e) upper layer transport is blocked for net transport above ~$0.3x10^5$ m^3 s^{-1}. For the bottom layer transport the respective value is ~$0.2x10^3$ m^3 s^{-1}.

North of the Sound the scatter of data demonstrates that this area is subject to oceanographic conditions originating from the Kattegat (e. g. transport appears rather stochastic and not fully constrained by the straits dynamics) and therefore for the same net transport different combinations of surface and bottom transport are possible. The upper and bottom layer transport across the southern sections in the Sound are much more constrained by the straits physics and therefore the scatter of data is smaller. Nevertheless, the scatter of data is too big to define a threshold value for blocking either surface or bottom transport in the Sound. It is interesting to see that this scatter increases in some sections (Fig. 14f), but only under the inflow situation. This is similar to the case in the Great Belt (Fig. 14h), but much more clearly pronounced in the Sound asymmetric response. This is in qualitative agreement with the results shown in Fig. 12 and previous analyses of Jakobsen (1995) and Stanev (2015).

In conclusion, the scatter of individual transports is usually larger at both ends of the strait, while in the middle of the straits the relationships are reminiscent of the “canonical” relationship known for other straits. Although the simulated two-layer transport is similar to other strait cases, there are specific asymmetries in the Baltic Sea straits. The relationships between the net transport and transport in the surface and bottom layer are not unique, thus deviating from simple theoretical estimations.

8. Fine versus coarse- resolution simulations

With a resolution of 500 m in the NBTZ, the cross-sectional areas in the Great Belt and Sound are 122300 m² and 68800 m², respectively (121100 m² and 73000 m² in CR). The TR is 1.78 (1.65 in CR) thus it changed relatively little (~8 percent) with changing the resolution. This small change is at least partially due to the fact that the DEM used in the CR and E-500 is the same. However, as seen in Fig. 3, the straits are resolved in the CR with only a few vertical columns.

Therefore, although the changes of topography in the CR and E-500 were relatively small, the different horizontal resolution led to substantial effects, which will be considered below.

In the Great Belt, the mean magnitude of barotropic transport during October 2014-May 2015 changed from 9.32 x 10^4 m^3/s in the CR to 8.49 x 10^4 m^3/s (in E-500). The respective numbers for the Sound are 4.66 x 10^4 m^3/s and 4.08 x 10^4 m^3/s. The averaged TR between the simulated transports in the two straits for the same period changed from 2.70 (CR) to 3.0 (E-500). The analysis of transport properties in the two straits (similar to what has been shown in Fig. 13 for CR, and in Fig. S4 for the E-500) demonstrated that the changes in the model resolutions affected the TR-distribution curves (compare the histograms in Fig. 13 and Fig. S4). The inflow histogram in E-500 tends to a Gaussian type, which can be interpreted as a trend to lower asymmetry between strait exchanges in the case of coarser resolution of straits. The temporal evolution of the distribution of the TR (compare Fig. 13 g and Fig. S4g) gives another illustration of the differences between the two experiments. Each time slice in these plots represents a normalized histogram of the TR analyzed for a period of three days. The secondary maximum in the histograms during outflow conditions (Fig. S4d) is clearly seen for small and negative values of TR (Fig. S4g). Although the transport in the straits does not change drastically in the two experiments, their relative distribution and correlation is strongly affected by the horizontal resolution.

The areal distribution of correlation between the transport in the straits and sea level in E-500 almost repeats the pattern shown in Fig. 12 e. The difference between the respective correlations in two experiments can be used to identify areas where changes in the dynamical balances occur. This difference does not exceed several percent (Fig. 12f), however its pattern is not trivial. Notably, far from the straits, where the horizontal resolution in the two experiments is the same, the areal distribution of this correlation is different. The coarser resolution of narrow sections in E-500 results in an overall decrease of correlation in the Kattegat. The maximum decrease is along the western coast where the tidal range is larger (Stanev et al., 2015). South of the straits the correlation increases in E-500 (in comparison to CR) and the difference pattern in Fig. 12f depicts approximately the propagation pathway of the North Sea mixed water. The correlation pattern shows strong sensitivity to horizontal resolution in narrow channels, e.g. between the

748 Langeland and the Fyn (Sio Sound) and in the area around Darss Sill. In both areas, Fig. 12f
749 shows reversals of correlation and small-scale patterns demonstrating that dynamical changes
750 can be locally strongly affected by the resolution. In particular, the response to changed
751 resolution in the Sound could explain at least some of the differences in the water mass
752 transformation and propagation towards the Gotland Basin.
753
754 Differences between the CR and E-500 originate from the areas where horizontal resolution has
755 substantially been changed, as can be seen in the enlarged diagrams in Fig. S3 and Fig. S5.
756 Inflow salinities are higher in the CR (compare Fig. S3b, f and S5b, f) and in the Sound the core
757 of high salinity water is very pronounced in the CR (see the difference between Fig. S3f and
758 S5f). In the outflow situations shown in these figures, salinity is lower in the CR. Of particular
759 importance to illustrate the differences between the two experiments is the comparison of
760 vorticity in the straits, which yields information about the velocity shear. In the Sound, these
761 differences are much clearer during inflow events (compare Fig. S3h and Fig. S5h). The
762 respective outflow situations (Fig. S3g and S5g) show much better similarity. The conclusion is
763 that with finer resolution in the CR (compare Fig. S1b and S1d), velocity shear along straits'
764 coasts is better resolved, which changes the patterns of velocity and salinity.
765
766 In several of the illustrations (Figs. 6, 7, 10, 11) simulations with E-500 were shown next to ones
767 from the CR, but were not commented on because the analyses were focused on physical
768 interpretation of results. In the following, we will present briefly the major differences between
769 the CR and E-500. Overall, the fine resolution model overestimates bottom salinity in Arkona
770 Basin (Fig. 6a). Before the MBI, bottom salinity in the Bornholm Basin simulated in the CR was
771 closer to the observed one, while after the MBI observed data lay between E-500 and the CR
772 simulations (Fig. 6c). In the Stolpe Channel and further down to the Gotland Basin, the quality of
773 CR simulations was better (notice the different colors in Fig. 6d corresponding to individual
774 experiments). SSS values were much closer in the two models than the bottom ones. Obviously,
775 changing the resolution affects the properties of bottom layers.
776
777 The panels on the right hand side of Fig. 10 are based on the results from E-500. Qualitatively,
778 both simulations look similar, but differences on both sides of the straits are also clearly seen.

779 The low sea level in the area of Skagerrak is further reduced in the E-500 simulations.
780 Furthermore, the positive SSS anomaly is more pronounced in the North Sea in E-500. These
781 changes are explained by larger mixing in the straits (overturning of water) during extreme
782 situations bringing bottom water closer to the sea surface, which further propagates in the
783 direction of the North Sea (compare also Fig. S3a, e and Fig. S5a, e). After the MBI the
784 freshening trend in E-500 is stronger. These results prove that the resolution in the straits can
785 affect remote areas.
786
787 The differences between two models are more obvious in the Baltic Sea where the bottom
788 salinity anomaly is much clearer in the CR. In E-500, the signal almost does not reach the
789 Gotland Basin. This is seen from the comparison between Fig. 7h and Fig. 7i and the data (Fig.
790 7g) and supports the conclusions from analysis of Fig 6. With more realistic bottom topography
791 and better resolution of the narrow flows, the penetration of saltier water in the straits simulated
792 in the CR is larger and their accumulation in the Arkona Basin and Bornholm Deep reservoir
793 provides enough source water to be “pushed” via the Stolpe Channel in the direction of the
794 Gotland Basin under favorable conditions (compare Fig. 10e and Fig. 10f). This is in line with
795 the analysis of Janssen (2002) who stated that ventilation of the Gotland Basin is only possible
796 when water mass characteristics in the Arkona Basin are beyond a critical value enabling
797 sufficient salty water to reach the Bornholm Basin. Obviously, the CR fulfilled these
798 requirements.
799
800 More complete presentation of the agreement between the two models is shown in Fig. 11. SSS
801 and bottom salinity along section lines in Fig. 2 simulated in the two experiments (Fig. 11b, c)
802 agree with each other, as was also the case with the larger-scale analysis in Fig. 10. Although
803 SSS patterns qualitatively agree and the bottom salinity shows similar appearances of salt
804 intrusions, the magnitude of the variability is different in the two models, particularly in the
805 Sound. At all analyzed stations, the CR gives larger salinity values. More detailed analysis shows
806 larger differences, e.g., in station Viken, where E-500 shows lower amplitudes of oscillations. In
807 this location the position of the salinity front shifts under different resolutions, which explains
808 the relatively larger salinity differences there (D=0.73). This changing skill of SCHISM in
809 different areas depending upon the resolution in the straits (Fig. 6 and Fig. 7) gives a motivation

to further address the parameterizations used to more reasonably simulate the penetration of the mixed North Sea water along its way from the Kattegat down to the Gotland Basin. Obviously, the problem with realistic propagation of bottom water could not be resolved with the increased resolution in the straits alone.

9. Conclusions

One basic idea behind this research was to use results from numerical modelling to address different issues of straits physics and dynamics of interconnected basins. This approach is justified by the fact that observations are not available over large areas and for sufficiently long periods with the needed resolution. An unstructured-grid model was presented, which overcame some deficiencies in past studies caused by the coarse resolution of the two-layer exchange in the straits and/or not using two-way coupling between the general circulation of interconnected basins and straits physics. Analyses gave a closer look at the impact of ultra-fine resolution scales, e.g., between 100 and 500 m. The extensive validation against available observations demonstrated a very good model skill giving sufficient credibility to simulations as 4D representation of dominant processes. We used these synthetic data to explain the key (and different) role of individual Baltic Sea straits and the temporal and spatial variability of their dynamics.

The realism of the model was first demonstrated with respect to the transport in the straits and the variability of sea levels at two ends of the straits. The volumetric transport showed a very good skill, revealing the leading role of the balance between along-strait pressure gradient and bottom friction. Furthermore, the consistency between basin-scale and strait-scale dynamics appeared crucial for the quality of the simulated gravity flows and basin-scale baroclinic dynamics. The model appeared capable of capturing the change of thermohaline characteristics of the North Sea waters penetrating into the Baltic Sea during the MBI along their way over the sills and in the small regional sub-basins. The timing of arrival of mixed North Sea water at several observational locations was accurately forecasted. The penetration of the bottom salinity signal into the Gotland Basin matched the observed one, particularly well up to Stolpe Channel.

There are number of geophysical specificities which have been revealed from the simulations. The Sound appeared as an area where extreme vertical mixing changes vertical stratification and strongly affects the propagation properties of gravity currents (in the Baltic Sea) and surface plume (in the North Sea). While the former can be expected, the fate of the surface plume in the North Sea was not so trivial. This plume was seen as alternating positive and negative anomalies, which propagated to the west. It was demonstrated that the Drogden Sill played the role of the generator of large salinity anomalies (mixer because of shallow depths). These anomalies propagated in either direction (depending on the alteration of the straits transport) as surface plumes in the North Sea and bottom plumes in the Baltic Sea.

Substantial differences between short-term variability during inflow and outflow situations were identified. The inflows were characterized by multiple pulses and large oscillations in transport and salinity, while the outflows showed smoother changes. During periods of strong currents, the flow in the straits was unidirectional. Decreasing the magnitude of the net transport below some critical value, caused the transport to become two-directional. However, the appearance of two-layer transport was quite diverse, which was seen by the different pairs of surface and bottom flows corresponding to the same net transport. The magnitude of net flow beyond which one of the two-way currents was blocked was also not unique. This “ambiguity” was different in different straits and at different locations in the straits. In the interior of the straits, the two-layer transport tended to the “canonical” one known from theory (Oguz et al., 1990). North and south of the straits the scatter of transport pairs (surface and bottom ones) increased because these areas were exposed to oceanographic conditions. Furthermore, the two-layer exchange was not symmetric for inflow and outflow conditions (non-canonical behavior under the inflow situation).

The three individual straits revealed very different dynamics. Saltier mixed North Sea water showed much longer excursions in the Great Belt, both in the surface and bottom layers than in the surface layers of the Sound. Nevertheless, during the MBI of 2014-2015, the salinity signal in the Bornholm Basin reflected water originating from the Sound.

Although there are concepts about the *causality of inflow events* (Svansson, 1959; Jakobsen et al., 2010; Schimanke et al., 2014) the contribution of the sea level changes in the Baltic Sea and North Sea for transports in the straits have not been previously quantified. The model simulations were reminiscent of similar results for the Black Sea-Mediterranean Sea system (Volkov et al., 2016), i.e. the major driver was the forcing from the outside basin. However, inflows were strongly dependent on the sea level in the central Baltic Sea, which supported the existing concepts (Lass and Matthäus, 1996). The correlation between net straits transport and sea level revealed an overall anti-symmetric pattern; the transition from positive to negative values made it possible to identify the natural (physical) boundaries between the North Sea and Baltic Sea.

The interdependence of the exchange in the individual straits does not fully conform to the simple idea that transports in the straits are linearly proportional, the coefficient being the ratio between the smallest cross-sectional areas. In fact, the transport in the Sound is smaller, which reveals the stronger frictional control there. We demonstrated that there are very complex relationships between transports in the two straits partially manifested by the large magnitudes of oscillations (comparable to the mean values). The coefficient of linear regression between transports in the Sound and Great Belt increased during the MBI-dominated cases, demonstrating the role of the Sound as a pathway for North Sea waters associated with extreme events. Furthermore, the transport in the Great Belt lags the one in the Sound, which was explained as a result of the Sound being closer to the inflowing waters following the eastern coast of Kattegat.

The changes in the model resolutions (from fine to ultra-fine) affected the strait exchange. The almost Gaussian-type histograms in the coarser simulation (E-500) can be interpreted as a trend to lower asymmetry between strait exchanges in the case of coarser resolution of straits. In the Sound the position of the salinity front shifts under different resolutions. Overall, the fine resolution model (CR) overestimated slightly bottom salinity in the Arkona Basin. However, in the Stolpe Channel and further down to the Gotland Basin, the CR simulations were superior. Comparisons between the CR and E-500 proved that the resolution in the straits affects remote locations in both inter-connected basins. The improvements due to using ultra-fine resolution appeared fundamental in the Baltic Sea, allowing more realistic simulation of the propagation of

the salinity signal down to the Gotland Basin. This was due to the fact that in the CR the penetration of saltier water in the straits was larger and its accumulation in the Bornholm Deep reservoir provided enough source water for the deep-ocean ventilation. It is questionable whether the increased resolution in the straits alone could fully solve the problem with realistic propagation of bottom water. Some further improvement of model skill could be achieved after a closer look at the physical parameterizations contributing to more accurate simulation of the penetration of the mixed water down to the Gotland Basin and its spreading there.

Acknowledgements

We acknowledge the German Federal Maritime and Hydrographic Agency (BSH), the German Weather Service (DWD) and Copernicus - Marine environment monitoring service (CMEMS) for the data made available for this study. SMHI made available river run-off data. We are grateful to V. Hues for making observations in Danish Straits available to us and to Julie Herman who edited the revised manuscript. This work has been supported by the BMBF-funded project 01DO17017: Cross-scale earth system processes and modelling. JP acknowledges support from the Copernicus project CEASELESS.

References:

Arneborg, L., V. Fiekas, L. Umlauf, and H. Burchard (2007), Gravity current dynamics and entrainment—A process study based on observations in the Arkona basin, J. Phys. Oceanogr., 37, 2094–2113.

Armi L (1986) The hydraulics of two flowing layers of different densities. J Fluid Mech 163:27–58

Armi L, Farmer DM (1988) The flow of Mediterranean Water through the Strait of Gibraltar. Prog. Oceanogr. 21:1–105

Borenäs K, Lundberg P (1986) Rotating hydraulics of flow in a parabolic channel. J Fluid Mech 167:309–326

931 Dukhovskoy, D. S., Morey, S.L., O'Brien, J.J., Martin,P.J., Cooper,C., 2009. Application of a
932 vanishing quasi-sigma vertical coordinate for simulation of high-speed deep currents over the
933 Sigsbee Escarpment in the Gulf of Mexico. Ocean Modell 28,250–265.
934 Farmer DM, Armi L (1988) The flow of Atlantic Water through the Strait of Gibraltar. Prog
935 Oceanogr 21:1–105
936 Feistel, R., Nausch, G., Wasmund, N. (Eds.), 2008. State and Evolution of Baltic Sea, 1952–
937 2005: A Detailed 50-year Survey of Meteorology and Climate, Physical, Chemical, Biological,
938 and Marine Environment. John Wiley & Sons, Inc., Hoboken, New Jersey, USA, ISBN 978-0-
939 471-97968-5.
940 Fennel,W., Seifert,T., Kayser,B., 1991. Rossby radii and phase speeds in the Baltic Sea. Cont.
941 Shelf Res. 11, 23–36.
942 Gräwe, U., M. Naumann, V. Mohrholz, and H. Burchard, Anatomizing one of the largest
943 saltwater inflows in the Baltic Sea in December 2014, *J. Geophys. Res.*, 120, 7676-7697, 2015.
944 Gustafsson, B. G. (2004). Sensitivity of Baltic Sea salinity to large perturbations in climate. Clim
945 Res, 27: 237–251.
946 Jakobsen, F.,1995.The major inflow to the Baltic Sea during January 1993. J. Mar. Syst. 6, 227–
947 240.
948 Jakobsen, F., Hansen, I.S., Ottesen Hansen, N.E., Østrup-Rasmussen, F., 2010. Flow resistance
949 in the Great Belt, the biggest strait between the North Sea and the Baltic Sea. Estuarine Coastal
950 and Shelf Science 87 (2), 325–332.
951 Janssen, F. (2002) Statistische Analyse mehrj¨ahriger Variabilit¨at der Hydrographie in Nord-
952 und Ostsee. M¨oglichkeiten zur Validation und Korrektur systematischer Fehler eines regionalen
953 Ozeanmodells. Dissetartion, University of Hamburg. 158 pp.
954 Janssen, F., Schrum, C., Backhaus, J. (1999). A climatological dataset of temperature and
955 salinity for the Baltic Sea and the North Sea. Deut. Hydrogr. Z.,supp. 9, 5–245.
956 Janssen, F., C. Schrum, U. Hübner, and J. O. Backhaus (2001). Uncertainty analysis of a decadal
957 simulation with a regional ocean model for the North Sea and Baltic Sea. Climate Research, 18:
958 55–62.
959
960 Kliem,N.,Nielsen,J.W.,Huess,V.,2006.Evaluationofashallowwaterunstructuredmeshmodelforthe
961 NorthSea–BalticSea.OceanModell15(1-2),124–136.doi:10.1016/j.ocemod.2006.06.003.

962 Kullenberg, G.,T. S. Jacobsen (1981). The Baltic Sea: an Outline of its Physical Oceanography.
963 Marine Pollution Bulletin. 12, 6, 183-186,
964 Laanearu, J., Lundberg, P., 2000. Topographic control of rotating deep water flow through the
965 combination of a sill and a horizontal constriction. Journal of Geophysical Research: Oceans
966 (1978–2012) 105 (C12), 28663–28669.
967 Lass, H.U., Matthäus, W., 1996. On temporal wind variations forcing salt water inflows into the
968 Baltic Sea. Tellus 48A, 663–671.
969 Lass, H.-U., Mohrholtz, V., 2003. On the dynamics and mixing of inflowing saltwater in the
970 Arkona Sea. Journal of Geophysical Research 108 (C2), 24/1-15.
971 Lehmann A (1995) A three-dimensional eddy-resolving model of the Baltic Sea. Tellus
972 47A:1013–1031
973 Lehmann, A., Myrberg, K., Höflich, K., 2012. Statistical approach to coastal upwelling in the
974 Baltic Sea based on the analysis of satellite data for 1990–2009. Oceanologia 54 (3), 369–393.
975 Leppäranta, M., Myrberg, K., 2009. Physical Oceanography of the Baltic Sea. Springer-Praxis,
976 Heidelberg, Germany, 378p.
977 Liljebladh B, Stigebrandt A (1996) Observations of the deepwater flow into the Baltic Sea. J
978 Geophys Res—Oceans 101:8895–8911
979 Mattsson, J (1996) Some comments on the barotropic flow through the Danish Straits and the
980 division of the flow between the Belt Sea and the Öresund, Tellus A: Dynamic Meteorology and
981 Oceanography, 48:3, 456-464.
982 Meier, HEM, Döscher R, Coward AC, Nycander J, Döös K (1999) RCO—Rossby Centre
983 regional Ocean climate model: model description (version 1.0) and first results from the hindcast
984 period 1992/93. Rep Oceanogr 26, Swedish Meteorological and Hydrological Institute,
985 Norrköping.
986 Meier, HEM, Döscher R and Faxén T (2003). A multiprocessor coupled ice-ocean model for the
987 Baltic Sea: Application to salt inflow. J. Geophys. Res. 108, NO. C8, 3273,
988 doi:10.1029/2000JC000521, 982 2003
989 Meier, HEM, Feistel, R., Piechura, J., Arneborg, L., Burchard, H., Fiekas, V., Golenko,
990 N., Kuzmina, N., Mohrholz, V., Nohr, C., Paka, V.T., Sellschopp, J., Stips, A., Zhurbas, V.,
991 (2006). Ventilation of the Baltic Sea deep water: a brief review of present knowledge from
992 observations and models. Oceanologia 48 (S), 133–164.

993 Meier, HEM, A. Höglund, · K. Eilola, · E. Almroth Rosell (2017). Impact of accelerated future
994 global mean sea level rise on hypoxia in the Baltic Sea. Clim Dyn) 49:163–172
995 Mohrholz,V., Naumann, M., Nausch, G., Krüger, S., and U. Gräwe, 2015. Fresh oxygen for the
996 Baltic Sea – An exceptional saline inflow after a decade of stagnation. J. Mar. Sys. 2015,
997 dx.doi.org/10.1016/ j.jmarsys.2015.03.005
998 Möller L (1928) Alfred Merz' hydrographishe untersuchungen in Bosphorus und Dardanellen.
999 Veroff. Inst. Meerskunde Univ., Berlin Neue Folge, A., 18, 284 pp
1000 Nielsen, M.H., 2005. The baroclinic surface currents in the Kattegat. Journal of Marine Systems
1001 55 (3), 97–121.
1002 O'Dea, E. J., Arnold, A. K., Edwards, K. P., Furner, R., Hyder, P., Martin, M. J., Siddorn, J. R.,
1003 Storkey, D., While, J., Holt, J. T., and Liu, H.: An operational ocean forecast system
1004 incorporating NEMO and SST data assimilation for the tidally driven European North-West
1005 shelf, Journal of Operational Oceanography, 5, 3–17, 2012.
1006 Pratt LJ, Lundberg PA (1991) Hydraulics of rotating strait and sill flow. Annu Rev Fluid Mech
1007 23:81–106
1008 Oğuz T, Özsoy E, Latif M, Sur HI, Ünlüata Ü (1990) Modeling of hydraulically controlled
1009 exchange flow in the Bosporus Strait. J Phys Oceanogr 20:945–965.
1010 Reissmann, J.H., Burchard, H., Hagen, R.F.E., Lass, H.U., Nausch, V.M.G., Umlauf, L.,
1011 Wieczorek, G., 2009. Vertical mixing in the Baltic Sea and consequences for eutrophication – a
1012 review. Progress in Oceanography 82, 47–80.
1013 Schimanke, S., C. Dieterich, and H. E. M. Meier (2014), An algorithm based on sea-level
1014 pressure fluctuations to identify major Baltic inflow events, Tellus, Ser. A, 66,
1015 doi:10.3402/tellusa.v66.23452.
1016 Schrum C (1997) A coupled ice-ocean model for the North Sea and the Baltic Sea. Sensitivity of
1017 North Sea, Baltic Sea and Black Sea to anthropogenic and climatic changes. In: Özsoy E,
1018 Mikaelyna A (eds) Sensitivity of North Sea, Baltic Sea and Black Sea to anthropogenic and
1019 climatic changes, NATO ASI Series, Environment Vol 27, Kluwer, Amsterdam, p 311–325
1020 Schrum, C., Alekseeva, I. and St. John, M. (2006): Development of a coupled physical–
1021 biological ecosystem model ECOSMO, J. Mar. Syst., 61(1–2), 79–99,
1022 doi:10.1016/j.jmarsys.2006.01.005,

Schrum C, Backhaus J (1999) Sensitivity of atmosphere-ocean heat exchange and heat content in the North Sea and the Baltic Sea. Tellus 51A(4):526–549

Stanev, E., X. Lu, S. Grashorn (2015), Physical processes in the transition zone between North Sea and Baltic Sea, Numerical simulations and observations. Ocean Modelling 93:56-74

Stanev, E.V., Grashorn, S. & Zhang, Y.J. (2017). Cascading ocean basins: numerical simulations of the circulation and interbasin exchange in the Azov-Black-Marmara-Mediterranean Seas system. Ocean Dynamics doi:10.1007/s10236-017-1071-2

Stigebrandt, A. (1983), A model for the exchange of water and salt between the Baltic and the Skagerrak, J. Phys. Oceanogr., 13, 411–427.

Svansson, A., 1959. Some computations of water heights and currents in the Baltic. Tellus 11 (2), 231–238.

Umlauf, L., Arneborg, L., 2009a. Dynamics of rotating shallow gravity currents passing through a channel. Part I: Observation of transverse structure. Journal of Physical Oceanography 39 (10), 2385–2401.

Umlauf, L., Arneborg, L., 2009b. Dynamics of rotating shallow gravity currents passing through a channel. Part II: Analysis. Journal of Physical Oceanography. 39 (10), 2402–2416.

Volkov DL, Johns WE, Belonenko TV (2016) Dynamic response of the Black Sea elevation to intraseasonal fluctuations of the Mediterranean sea level. Geophys Res Lett 43:283–290. doi:10. 1002/2015GL066876

Willmott, C.J., 1981. On the validation of models. Phys. Geogr. 2 (2), 184–194 .

Zhang,Y.,Ateljevich,E.,Yu,H-S.,Wu,C H.,Yu, J.C.S., 2015. A new vertical coordinate system for a 3D unstructured-grid model. Ocean Modell 85,16–31.

Zhang, Y.J., E.V. Stanev, S. Grashorn (2016a), Unstructured-grid model for the North Sea and Baltic Sea: Validation against observations. Ocean Modelling, 97, 91-108, ISSN 1463-5003, http://dx.doi.org/10.1016/j.ocemod.2015.11.009.

Zhang, Y., Ye, F., Stanev, E.V., Grashorn, S. (2016b) Seamless cross-scale modeling with SCHISM, Ocean Modelling, 102, 64-81.

List of figures

Fig. 1. Topography of the North Sea and Baltic Sea along with the notations used in text. Locations and transect line where analysis of model simulations and observations have been carried out are also shown. The numbers on transect line are kilometers from the beginning of section. The black box in the NBTZ identifies the position of Fig. 2.

Fig. 2. Topography of the NBTZ. Locations where analysis of model simulations have been carried out are also shown. The numbers on the transect lines are kilometers from the beginning of section-lines in the three straits (black in the Little Belt, red in the Great Belt, and blue in the Sound). The red solid lines indicate the position of the transects across the straits for which the transports are given in Fig. 14. Encircled red numbers identify these individual cross-sections. Positions of the ADCP-moorings (in Fig. 5) indicated by the black crosses with numbers and brackets are stations: 1) Drogden, 2) Østerrenden, 3) Vengeancegrund.

Fig. 3. Horizontal grid in the Sound in the CR (a) and in the E-500 experiment (c). The respective vertical grids are shown exemplarily in (b) and (d) along the section plotted by the thick black lines. For the position of (a) and (c), see the respective box in Fig. 2 in the area of Little Belt.

Fig. 4. Validation of the simulated sea level against gauge data in the stations Viken (a), Klagshamn (b), Visby (c) and Degerby (d); (e) shows the normalized (divided by their standard deviations) net transport in the Sound estimated by the numerical model and the sea level difference between the gauges of Klagshamn and Viken. Blue lines are used to show results from the model, the red ones correspond to observations. For presentation reasons all time series have been detided by applying a 1-day running average filter. The start of the MBI (4 December 2014) is indicated by the green vertical line.

Fig. 5. Comparison of along-channel velocities [m/s] against ADCP-observations in the Great Belt (a,c,e) and in the Sound (b,d,f). The beginning of MBI is indicated by green solid vertical line. The locations (in the titles of plots) are shown in Fig. 2.

1082 Fig. 6. Validation of simulated salinity. The positions of stations are given in Fig. 1. The legend
1083 explains the individual curves.
1084
1085 Fig. 7. Time versus depth diagram of observed (panels on the left) , simulated in the reference
1086 run (panels in the middle), and simulated in the coarse-resolution run (panels on the right)
1087 salinity in station Darss (a, b, c), Arkona, (d, e, f) and at station BY-15 (ICES data).
1088
1089 Fig. 8. Dynamics in the transition zone represented by the patterns of surface salinity and
1090 relative vorticity normalized by the Coriolis parameter. (a) and (c) show SSS during outflow and
1091 inflow periods, respectively. Time is shown in the title of each plot. (b) and (d) shows relative
1092 vorticity for tjhe same times. Rectangles identify the position of the insets shown in Fig. S3
1093
1094 Fig. 9. Salinity and turbulent kinetic energy along the blue-colored section line (Fig. 2) in the
1095 Sound. (a) and (c) show salinity during outflow and inflow period, respectively. Time is shown
1096 in the title of each plot. (b) and (d) show turbulent kinetic energy for the same times. The
1097 outflow-situation (upper plots) correponds to the period just before the MBI, the inflow one ,
1098 during the MBI, is shown in the bottom plots.
1099
1100 Fig. 10. Time versus distance along the section line in Fig. 1 diagrams of sea level in [m], (a, b),
1101 SSS anomaly (c, d) and bottom salinity anomaly (e, f). Panels on the left are from the control
1102 run, the ones on the right from the coarse-resolution one. The blue arrow shows the position of
1103 Drogden Sill, this is the shallow most depth in Fig, 7. Bornholm Deep is indicated by the red
1104 arrow.
1105
1106 Fig. 11 Time versus distance diagrams along the transect lines in Fig. 2.Each group of six panels
1107 depicts CR simulations (on the left) and E-500 ones (on the right) for the individual straits: upper
1108 two figures-Sound (So), the two figures in the middle – Great Belt (GB), the two bottom figures
1109 – Little Belt (LB). (a) is sea level, (b) is SST, (c) is bottom salinity.
1110
1111 Fig. 12: (a) Net volume flux [m^3/s] integrated over the three straits (positive in the direction of
1112 BalticSea) versus sea level difference [m] between the Kattegat (area averaged) and central

Baltic Sea (area averaged). A positive sea level difference means that sea level in the Kattegat is higher. (b) sea level difference [m] between the same areas as in (a) versus sea level [m] in the Kattegat. (c) sea level difference [m] between the same areas as in (a) versus sea level [m] in the central Baltic Sea. Data have been detided with a running average window of 1 day. (d) Temporal evolution of net transport in the Sound during the MBI in 2014-2015. (e) correlation map of volume flux integrated over the three straits [m^3/s] and sea level [m] in the NBTZ.(f) shows the difference between (e) and similar plot from E-500.

Fig.13.(a)Vertically integrated water transport through the Great Belt and Sound across the section lines 5 and 3, respectively (see Fig.2a for their positions) during October 2014 - May 2015. Negative values are towards the Baltic Sea. The ratio between the transports in the Great Belt and Sound is also given (green line) as a running average of 7 days. (b) is a scatter plot of the transport in the Sound versus the one in the Great Belt. The equation for the regression curve is also given; (c) and (d) show the distribution of the ratio between the transport in the Great Belt and Sound during the inflow and outflow conditions, respectively. The transport values in the Sound smaller than 9e3m3s-1havebeenexcluded; (e) is the same as (c) and (d) but for all conditions. (f) is the correlation of the water transport in the Great Belt and Sound as a function of time lag. (g) is the distribution of the ratio between the transport between the Great Belt and Sound, where each time slice represents a normalized histogram of this ratio analysed for a period of three days. The white solid line illustrates the average ratio of fluxes through Great Belt and Sound. The thick vertical lines in (a) and (g) indicates the beginning of the MBI in 2014.

Fig. 14. The volumetric flow rates across sections shown in (a) in the upper layer (red symbols) and bottom layer (green symbols) as a function of the net flow. Positive flows are from the North Sea to the Baltic Sea. The panels on the left are transports in the Little Belt, the ones in the middle in the Great Belt and the ones on the right in the Sound.

Supplementary figures

Fig. S1. Horizontal grid in the Sound in the CR (a) and in the E-500 experiment (c). The respective vertical grids are shown exemplarily in (b) and (d) along the section plotted by the thick black lines. For the position of (a) and (c), see the respective box in Fig. 2 in the area of Sound.

Fig. S2. Horizontal grid in the Sound in the CR (a) and in the E-500 experiment (c). The respective vertical grids are shown exemplarily in (b) and (d) along the section plotted by the thick black lines. For the position of (a) and (c), see the respective box in Fig. 2 in the area of Great Belt.

Fig. S3. Dynamics in the Great Belt (upper panels) and Sound (bottom panels) represented by the patterns of surface salinity and relative vorticity normalized by the Coriolis parameter. The individual figures are zooms of Fig. 8 in the straits. (a), (b) show SSS in the Great Belt during outflow and inflow periods, respectively. (c) and (d) shows relative vorticity in the Great Belt for the same times as (a) and (b). The same as in (a-d) is shown in (e-h) for the Sound.

Fig. S4. As Fig. 13 but from E-500.

Fig. S5. As Fig. S3 but for E-500D.

Figures

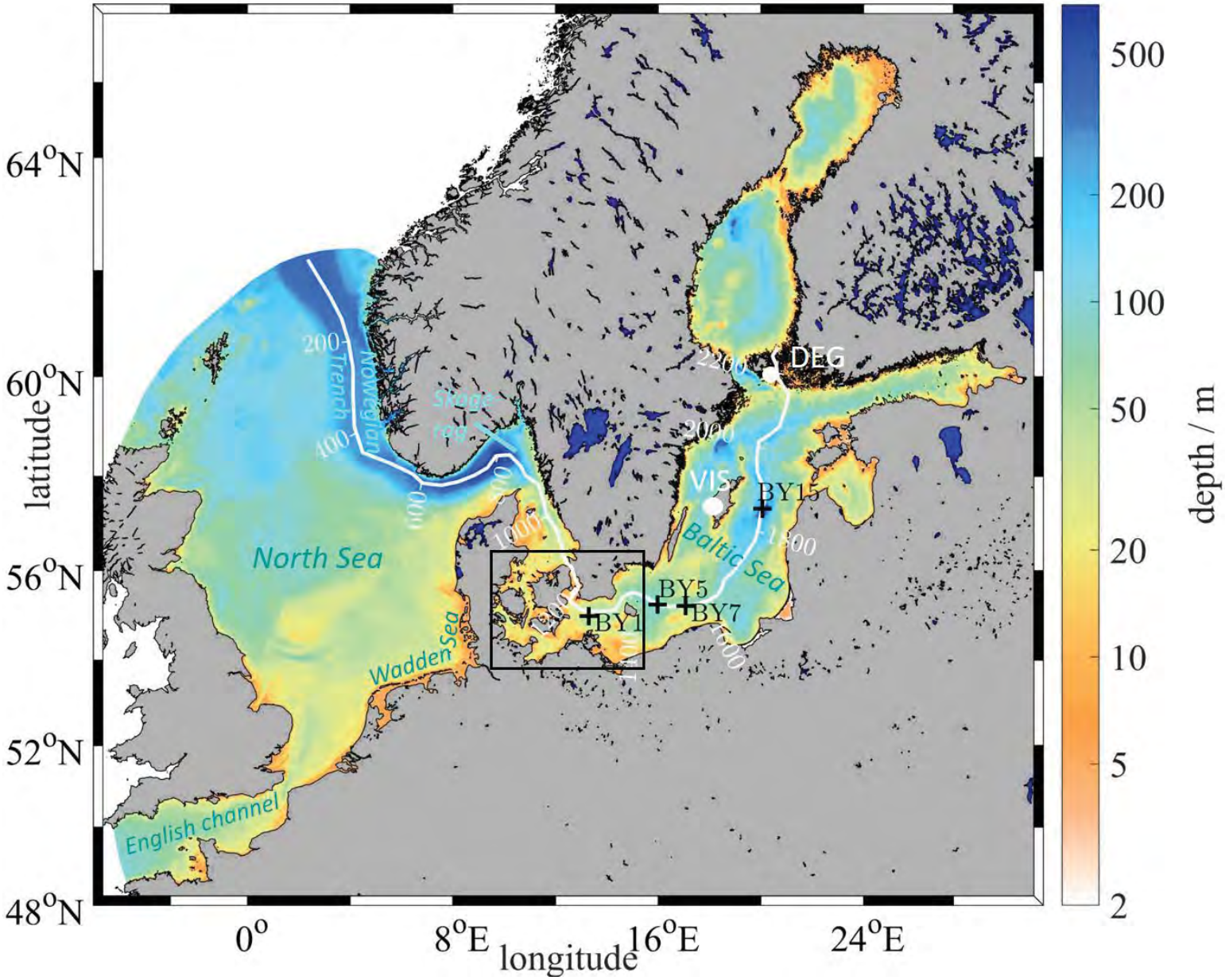
64°N
60°N
56°N
52°N
48°N
latitude
0°
8°E
16°E
24°E
longitude
depth / m
500
200
100
50
20
10
5
2
North Sea
Baltic Sea
Wadden Sea
English channel
Norwegian Trench
Skagerrak
DEG
VIS
BY1
BY5
BY7
200
400
600
800
1000
1200
1400
1600
2000
2200

Fig. 1.

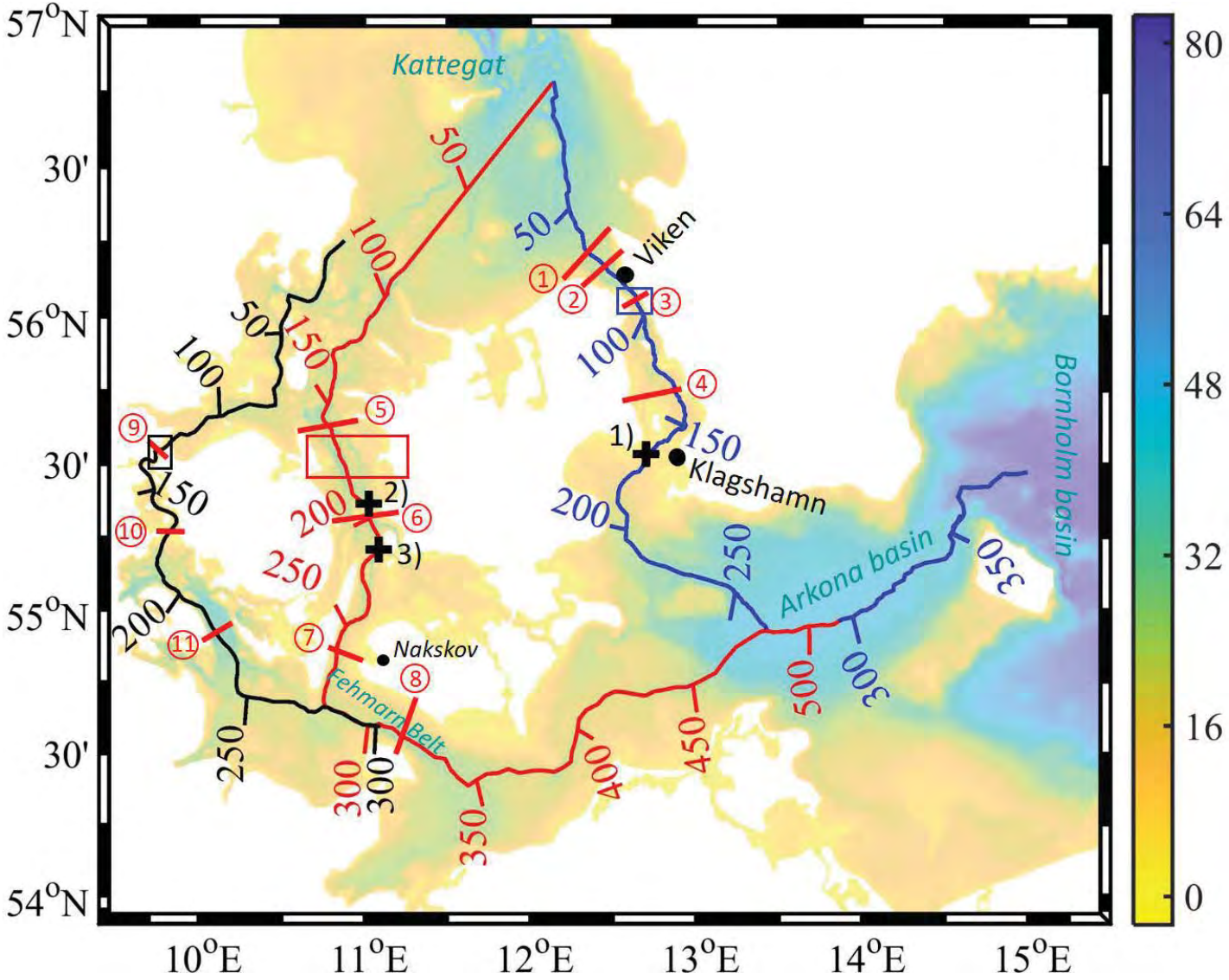
57°N
30'
56°N
30'
55°N
30'
54°N
10°E
11°E
12°E
13°E
14°E
15°E
Kattegat
Viken
Klagshamn
Nakskov
Fehmarn Belt
Arkona basin
Bornholm basin
80
64
48
32
16
0

Fig. 2.

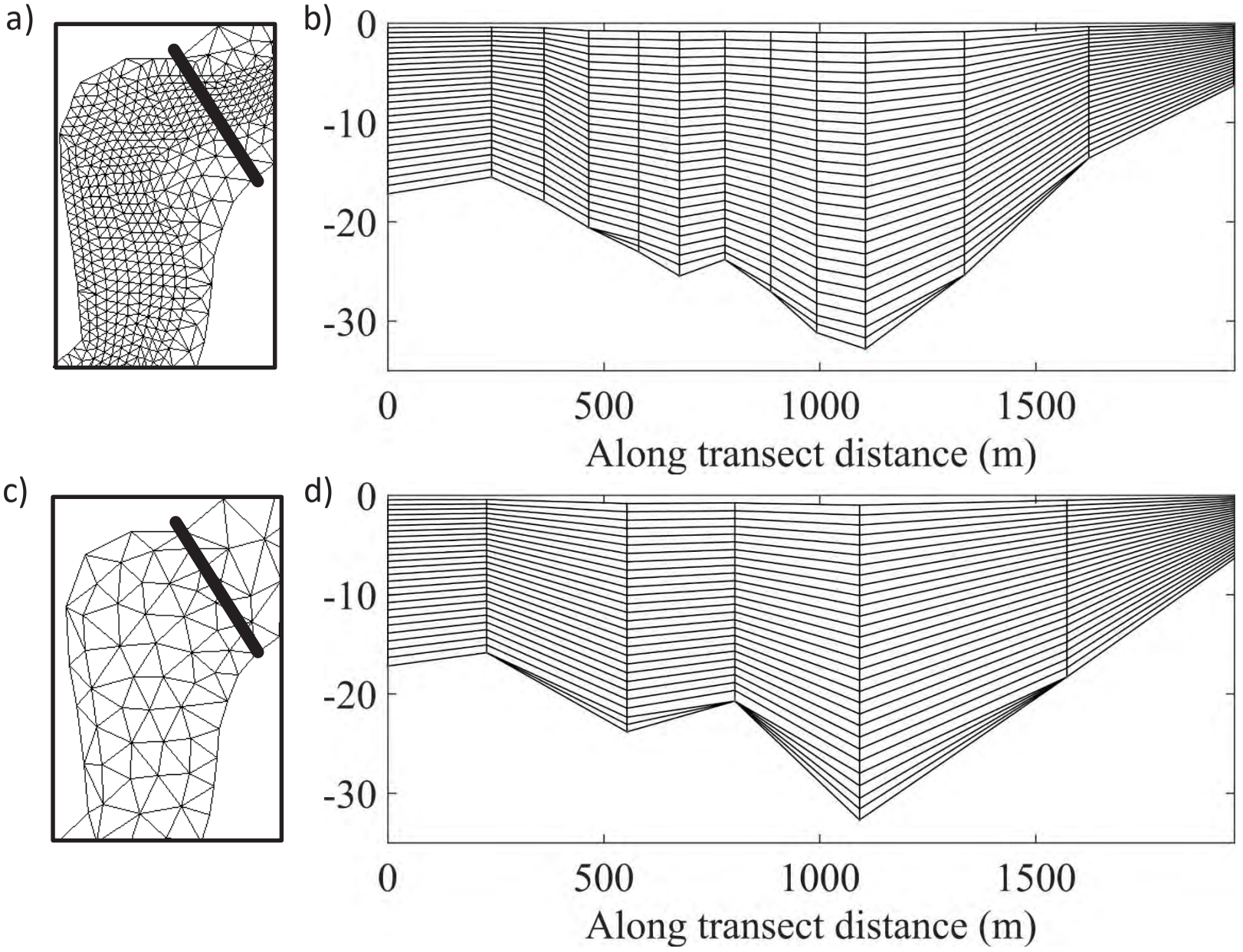
a)
b)
0
-10
-20
-30
0
500
1000
1500
Along transect distance (m)
c)
d)
0
-10
-20
-30
0
500
1000
1500
Along transect distance (m)

Fig. 3

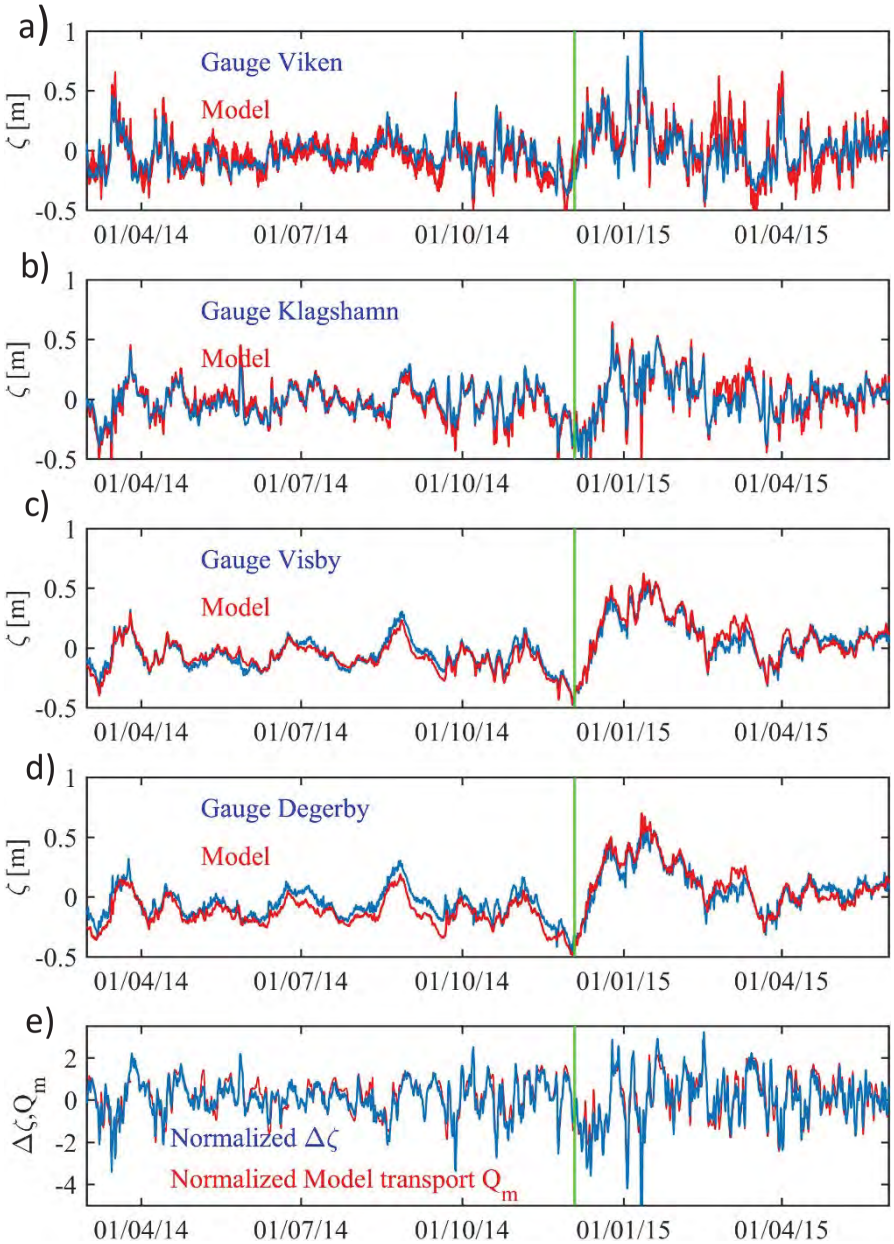
a)
Gauge Viken
Model
ζ [m]
b)
Gauge Klagshamn
Model
ζ [m]
c)
Gauge Visby
Model
ζ [m]
d)
Gauge Degerby
Model
ζ [m]
e)
Normalized Δζ
Normalized Model transport Q_m
Δζ,Q_m
01/04/14
01/07/14
01/10/14
01/01/15
01/04/15

Fig. 4.

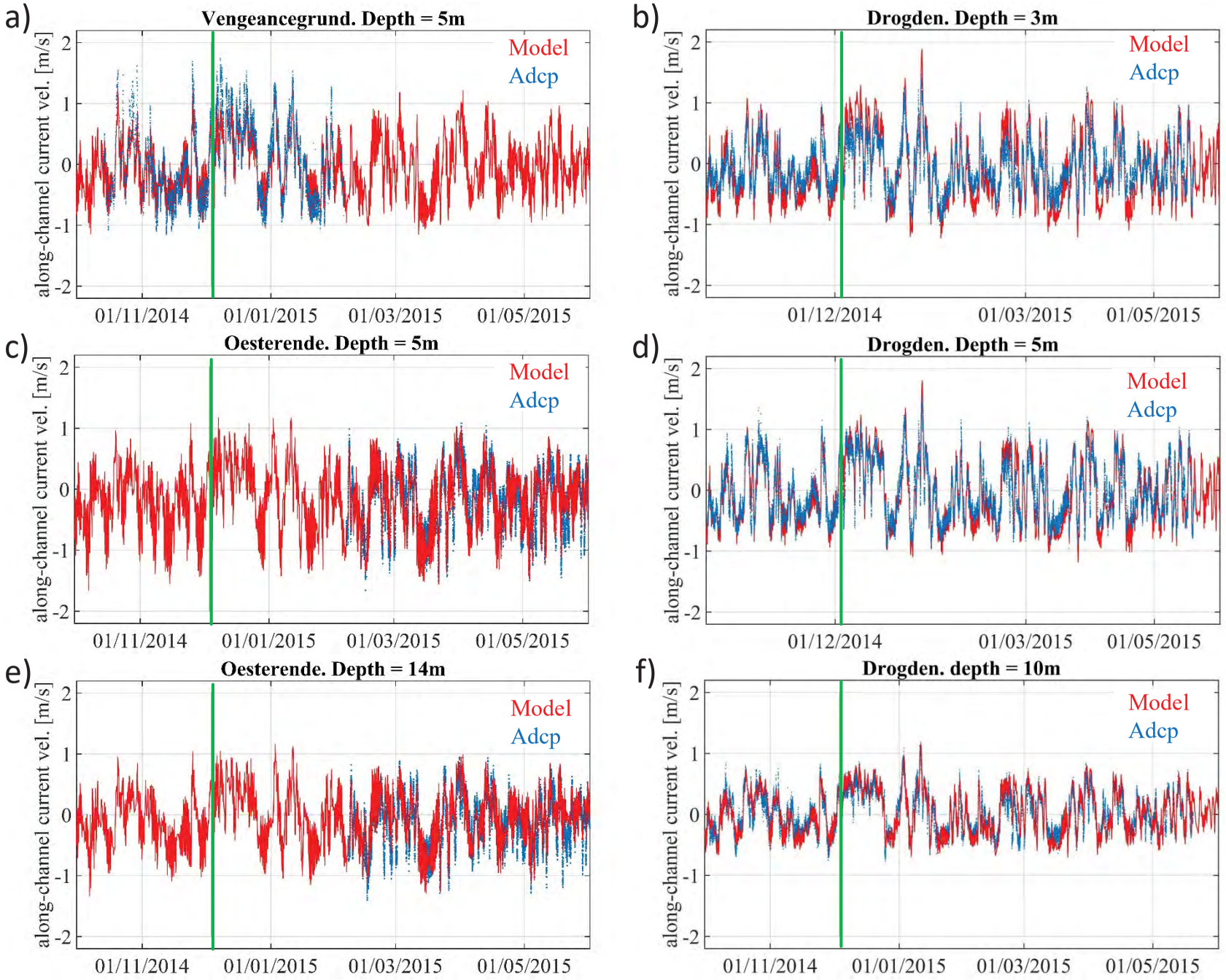
a)
Vengeancegrund. Depth = 5m
b)
Drogden. Depth = 3m
c)
Oesterende. Depth = 5m
d)
Drogden. Depth = 5m
e)
Oesterende. Depth = 14m
f)
Drogden. depth = 10m
Model
Adcp
along-channel current vel. [m/s]
2
1
0
-1
-2
01/11/2014
01/12/2014
01/01/2015
01/03/2015
01/05/2015

Fig. 5

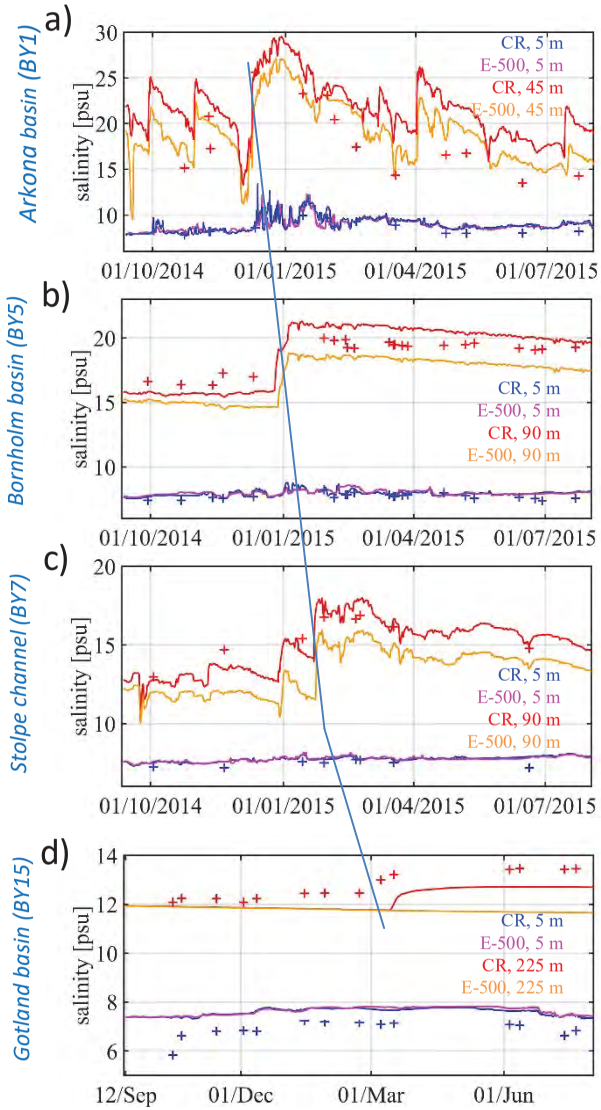
a)
Arkona basin (BY1)
salinity [psu]
CR, 5 m
E-500, 5 m
CR, 45 m
E-500, 45 m
01/10/2014
01/01/2015
01/04/2015
01/07/2015
b)
Bornholm basin (BY5)
CR, 90 m
E-500, 90 m
c)
Stolpe channel (BY7)
d)
Gotland basin (BY15)
CR, 225 m
E-500, 225 m
12/Sep
01/Dec
01/Mar
01/Jun

Fig. 6.

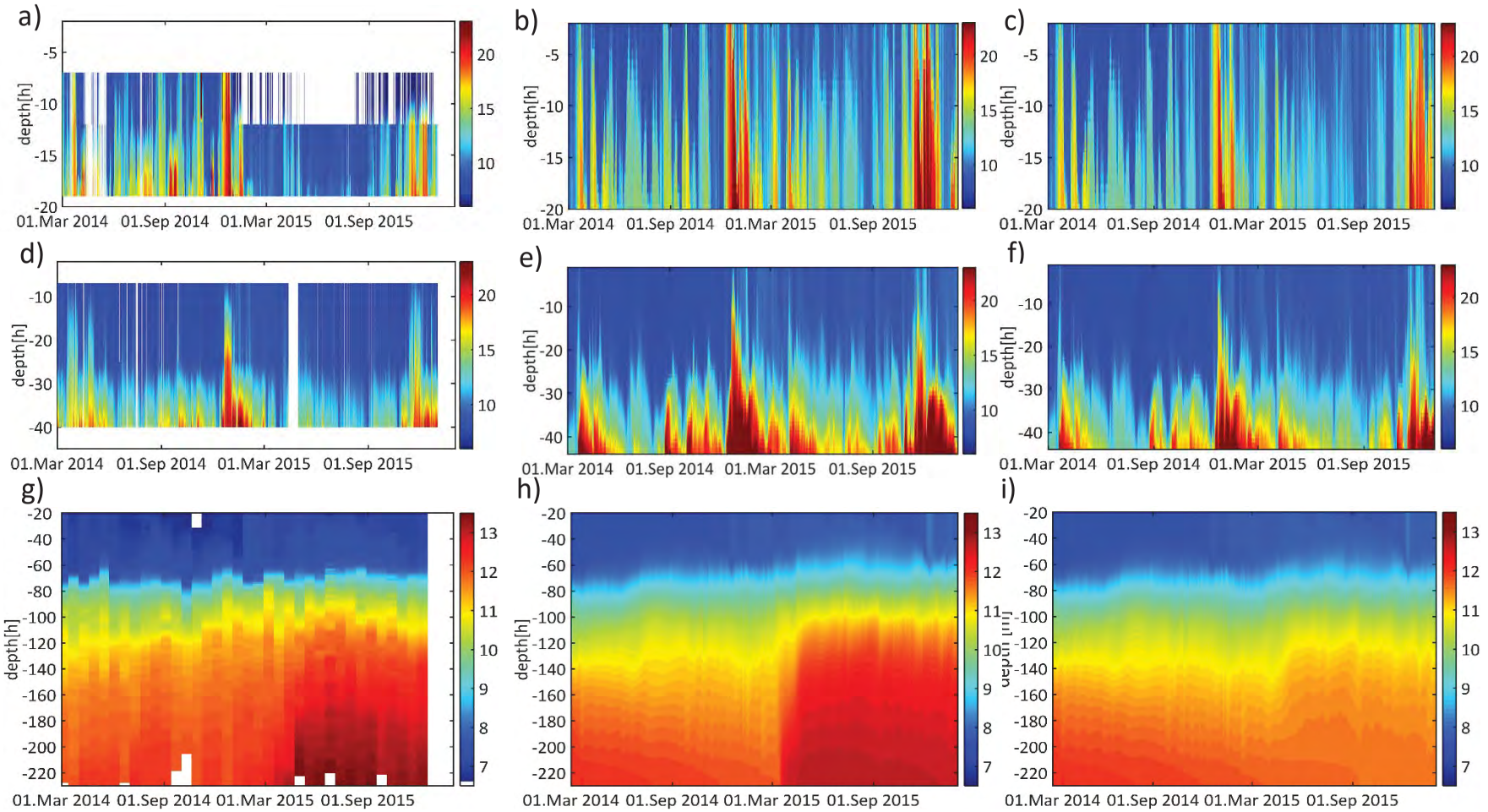
a)
b)
c)
d)
e)
f)
g)
h)
i)
depth[h]
01.Mar 2014
01.Sep 2014
01.Mar 2015
01.Sep 2015

Fig. 7.

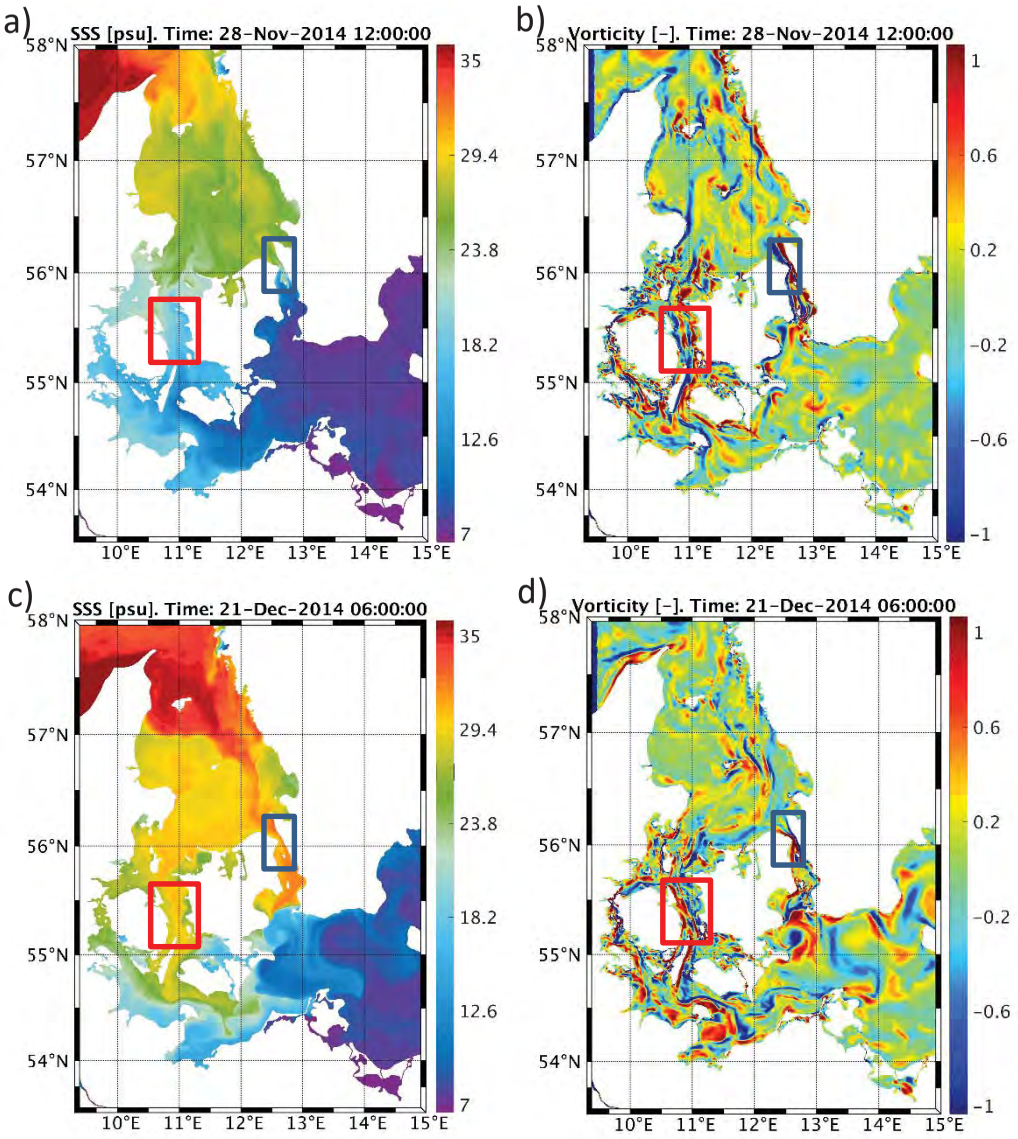
a)
SSS [psu]. Time: 28-Nov-2014 12:00:00
b)
Vorticity [-]. Time: 28-Nov-2014 12:00:00
c)
SSS [psu]. Time: 21-Dec-2014 06:00:00
d)
Vorticity [-]. Time: 21-Dec-2014 06:00:00
58°N
57°N
56°N
55°N
54°N
10°E
11°E
12°E
13°E
14°E
15°E
35
29.4
23.8
18.2
12.6
7
1
0.6
0.2
-0.2
-0.6
-1

Fig. 8.

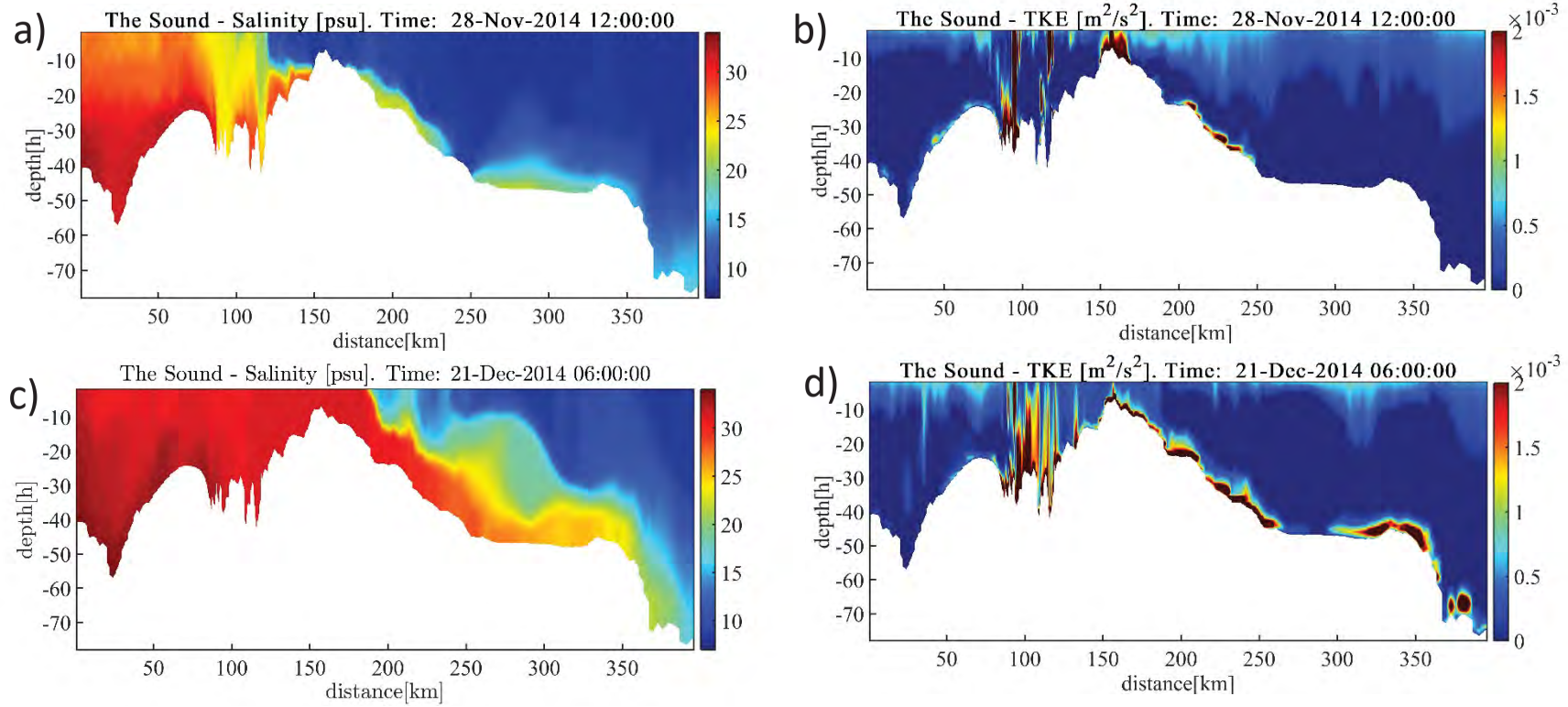
a)
The Sound - Salinity [psu]. Time: 28-Nov-2014 12:00:00
depth[h]
distance[km]
b)
The Sound - TKE [m²/s²]. Time: 28-Nov-2014 12:00:00
depth[h]
distance[km]
c)
The Sound - Salinity [psu]. Time: 21-Dec-2014 06:00:00
depth[h]
distance[km]
d)
The Sound - TKE [m²/s²]. Time: 21-Dec-2014 06:00:00
depth[h]
distance[km]

Fig. 9.

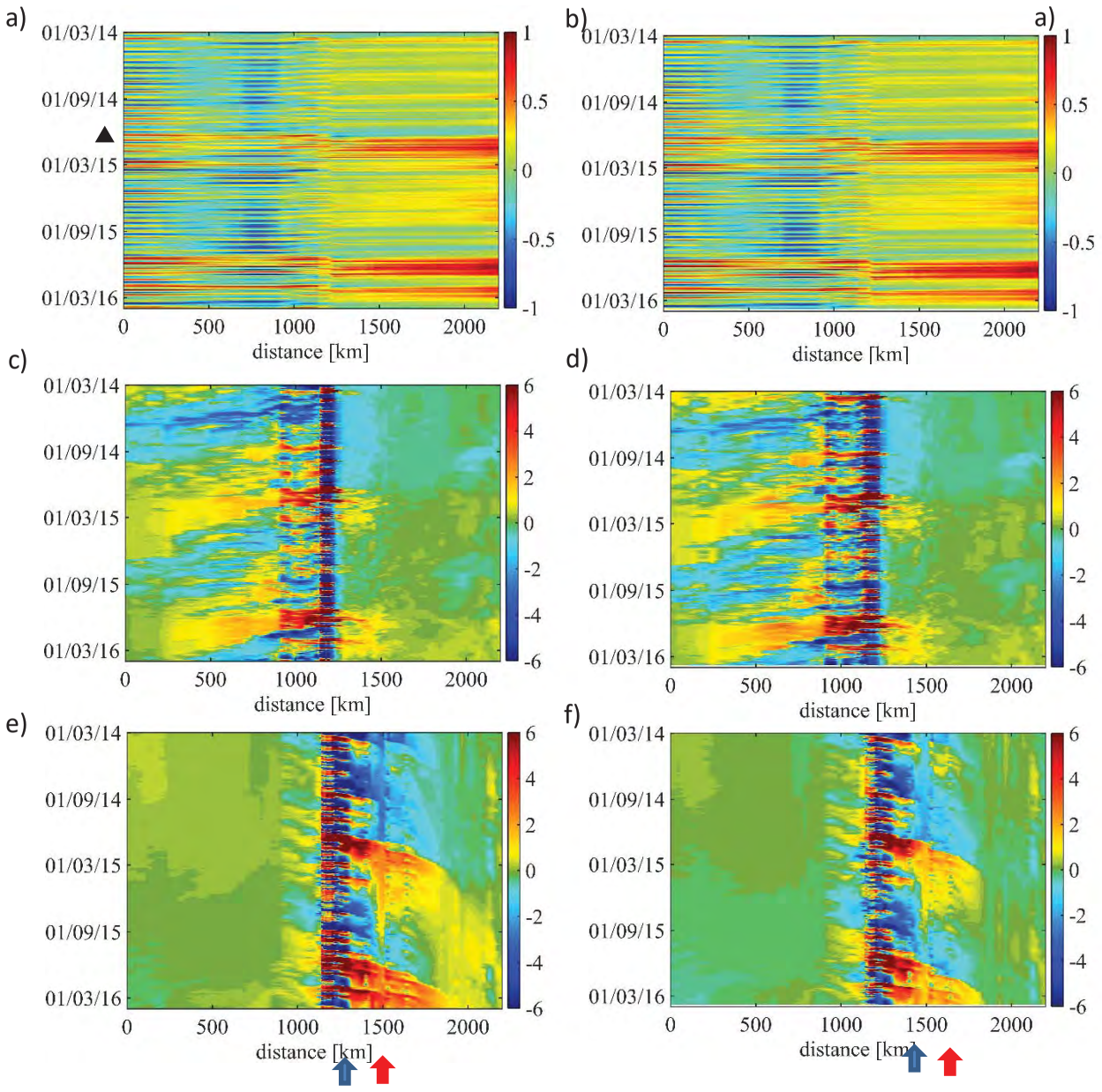
a)
b)
a)
c)
d)
e)
f)
01/03/14
01/09/14
01/03/15
01/09/15
01/03/16
0
500
1000
1500
2000
distance [km]
1
0.5
0
-0.5
-1
6
4
2
0
-2
-4
-6

Fig. 10.

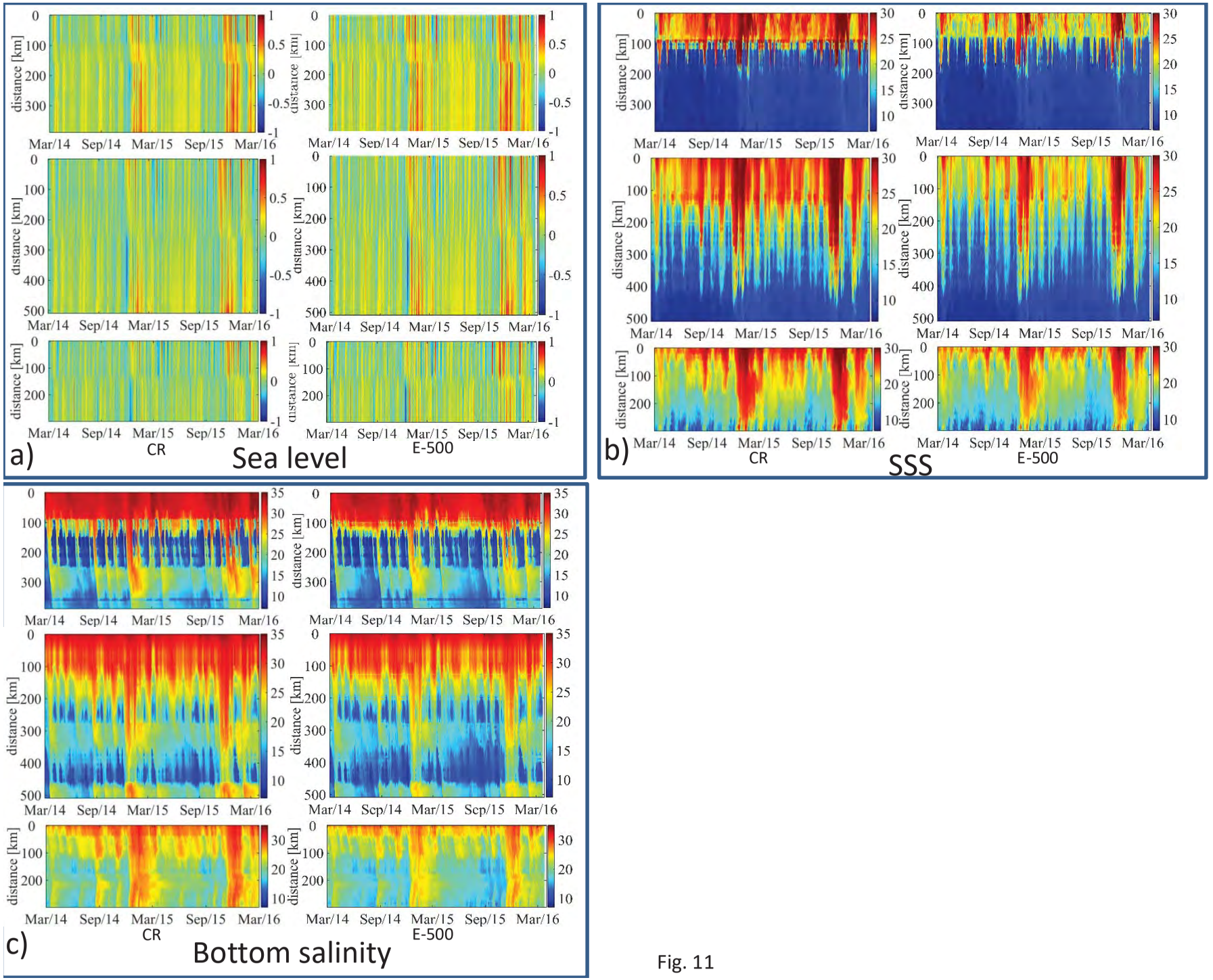
a)
Sea level
CR
E-500
b)
SSS
CR
E-500
c)
Bottom salinity
CR
E-500
distance [km]
Mar/14
Sep/14
Mar/15
Sep/15
Mar/16

Fig. 11

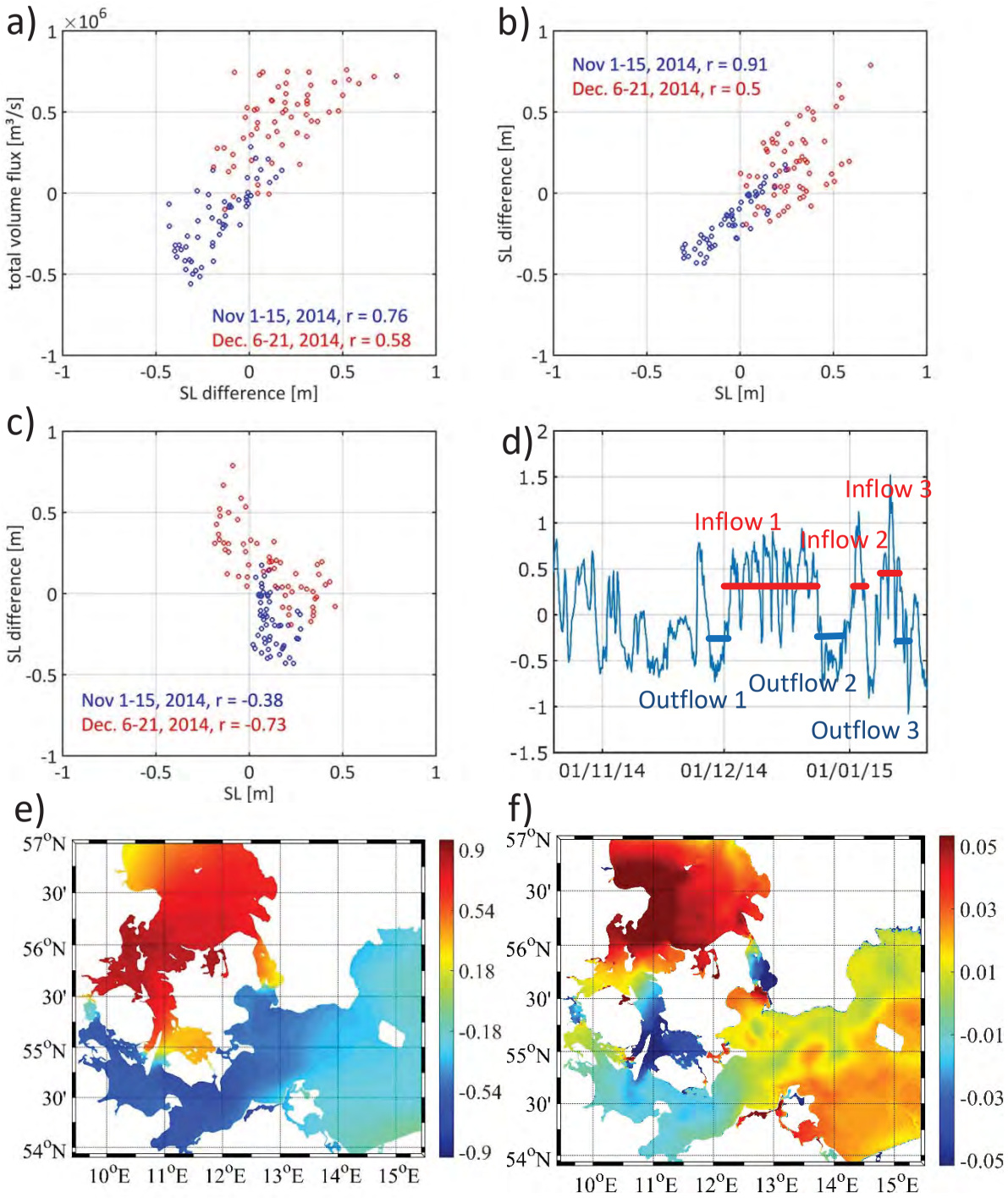
a)
×10^6
total volume flux [m^3/s]
SL difference [m]
Nov 1-15, 2014, r = 0.76
Dec. 6-21, 2014, r = 0.58
b)
SL difference [m]
SL [m]
Nov 1-15, 2014, r = 0.91
Dec. 6-21, 2014, r = 0.5
c)
SL difference [m]
SL [m]
Nov 1-15, 2014, r = -0.38
Dec. 6-21, 2014, r = -0.73
d)
Inflow 1
Inflow 2
Inflow 3
Outflow 1
Outflow 2
Outflow 3
01/11/14
01/12/14
01/01/15
e)
f)
57°N
30'
56°N
30'
55°N
30'
54°N
10°E
11°E
12°E
13°E
14°E
15°E
0.9
0.54
0.18
-0.18
-0.54
-0.9
0.05
0.03
0.01
-0.01
-0.03
-0.05

Fig. 12.

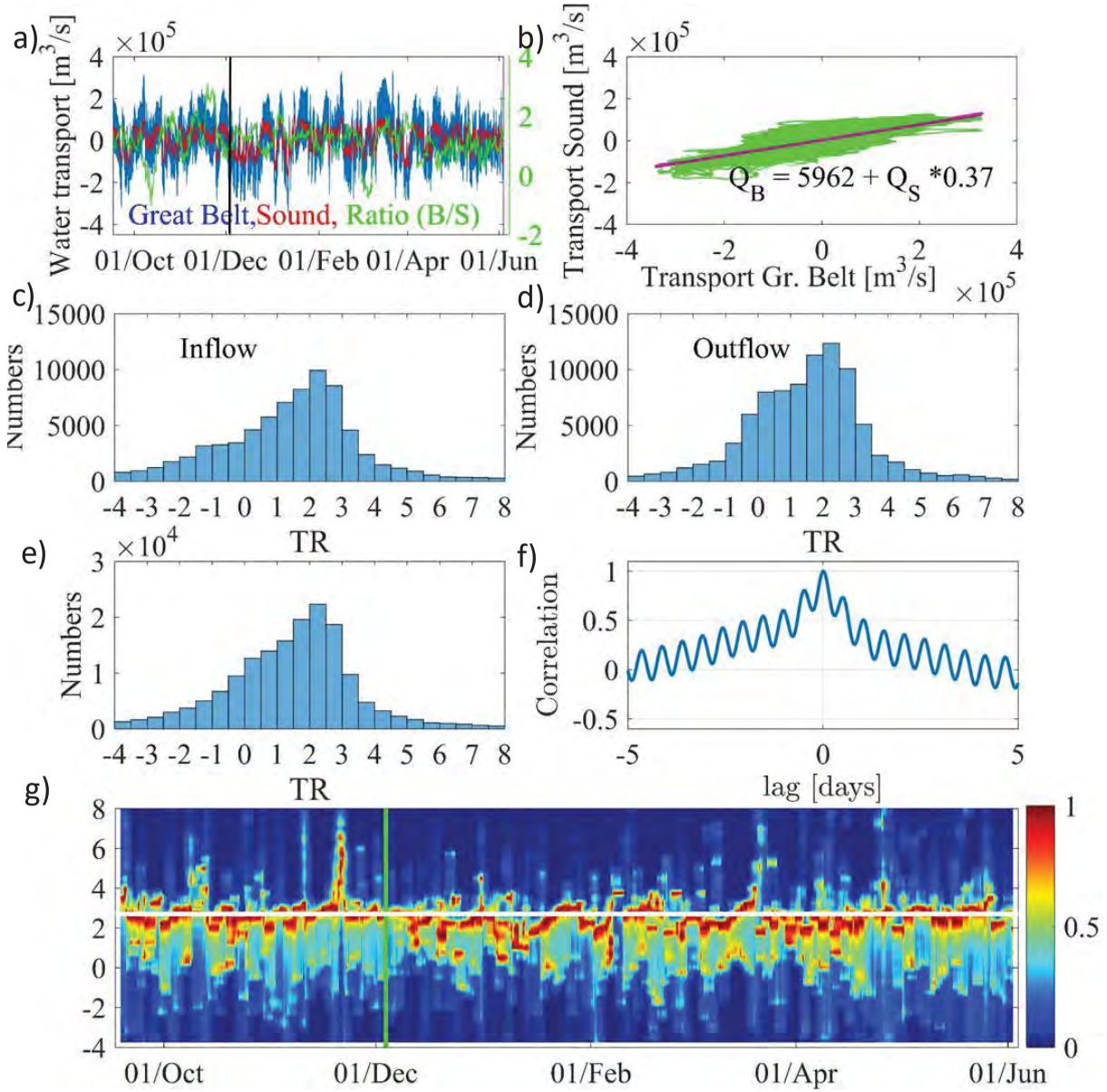
a)
Water transport [m3/s]
×10^5
Great Belt,Sound, Ratio (B/S)
01/Oct 01/Dec 01/Feb 01/Apr 01/Jun
b)
Transport Sound [m3/s]
×10^5
Q_B = 5962 + Q_S *0.37
Transport Gr. Belt [m3/s]
×10^5
c)
Inflow
Numbers
TR
d)
Outflow
Numbers
TR
e)
×10^4
Numbers
TR
f)
Correlation
lag [days]
g)
01/Oct
01/Dec
01/Feb
01/Apr
01/Jun

Fig.13.

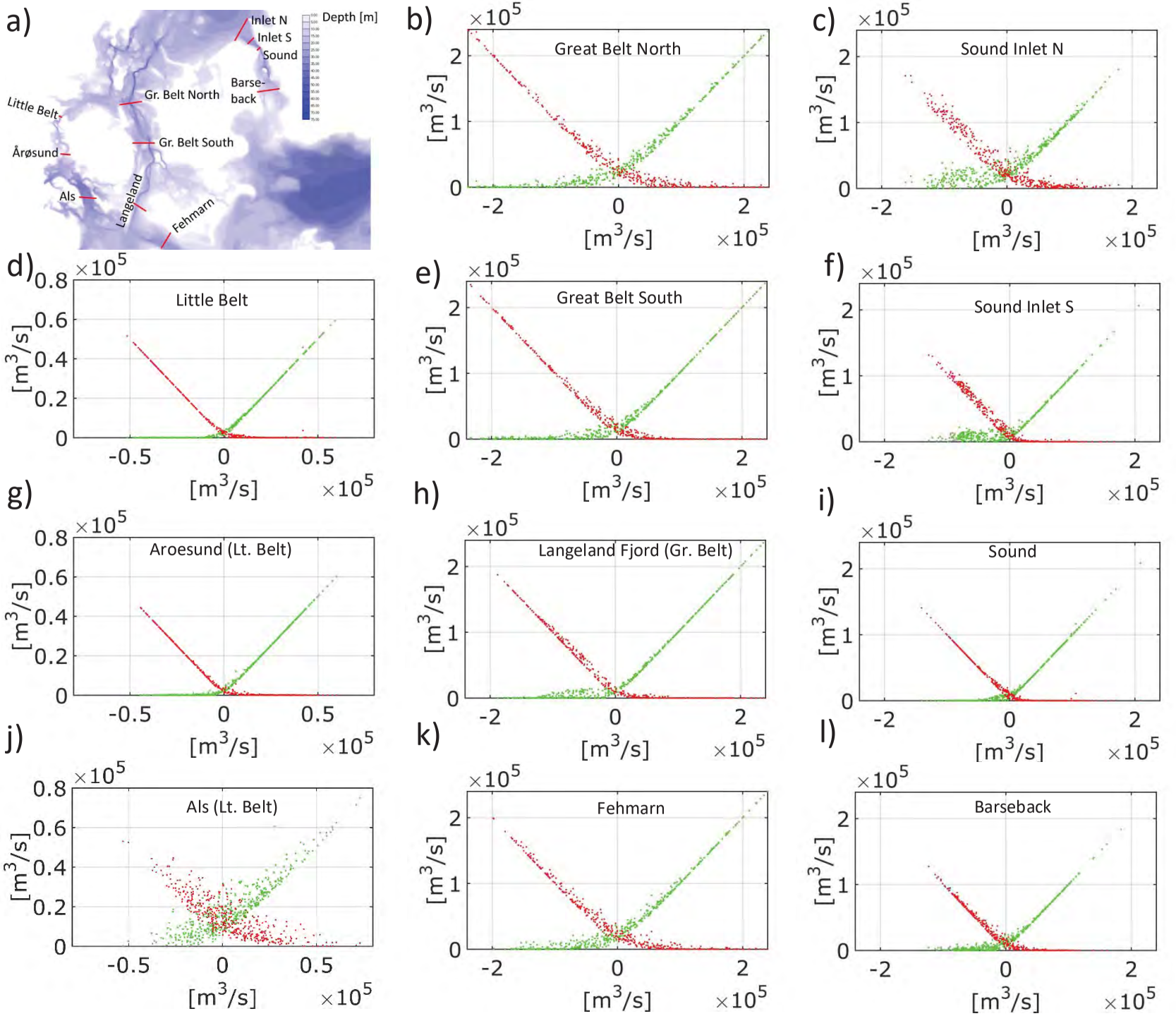
a)
Depth [m]
Inlet N
Inlet S
Sound
Barse-back
Gr. Belt North
Little Belt
Gr. Belt South
Årøsund
Als
Langeland
Fehmarn
b)
Great Belt North
c)
Sound Inlet N
d)
Little Belt
e)
Great Belt South
f)
Sound Inlet S
g)
Aroesund (Lt. Belt)
h)
Langeland Fjord (Gr. Belt)
i)
Sound
j)
Als (Lt. Belt)
k)
Fehmarn
l)
Barseback
[m3/s]
×10^5

Fig. 14.

Supplementary figures

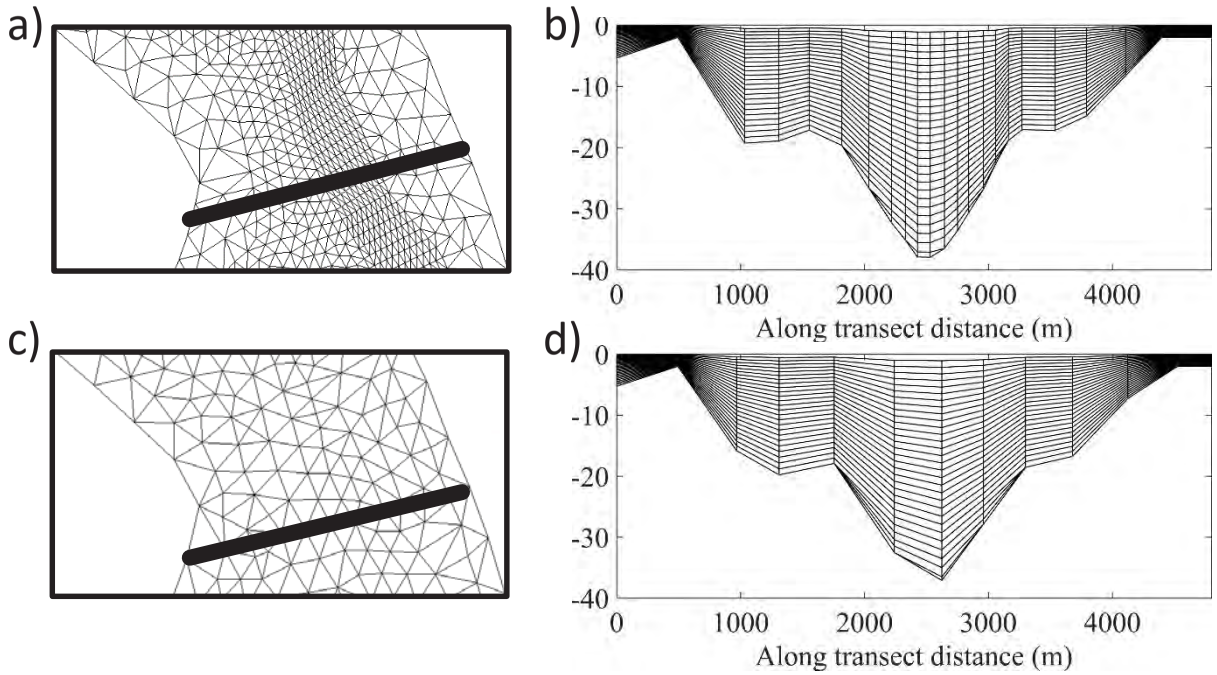
a)
b)
c)
d)
0
-10
-20
-30
-40
0
1000
2000
3000
4000
Along transect distance (m)
Along transect distance (m)

Fig. S1.

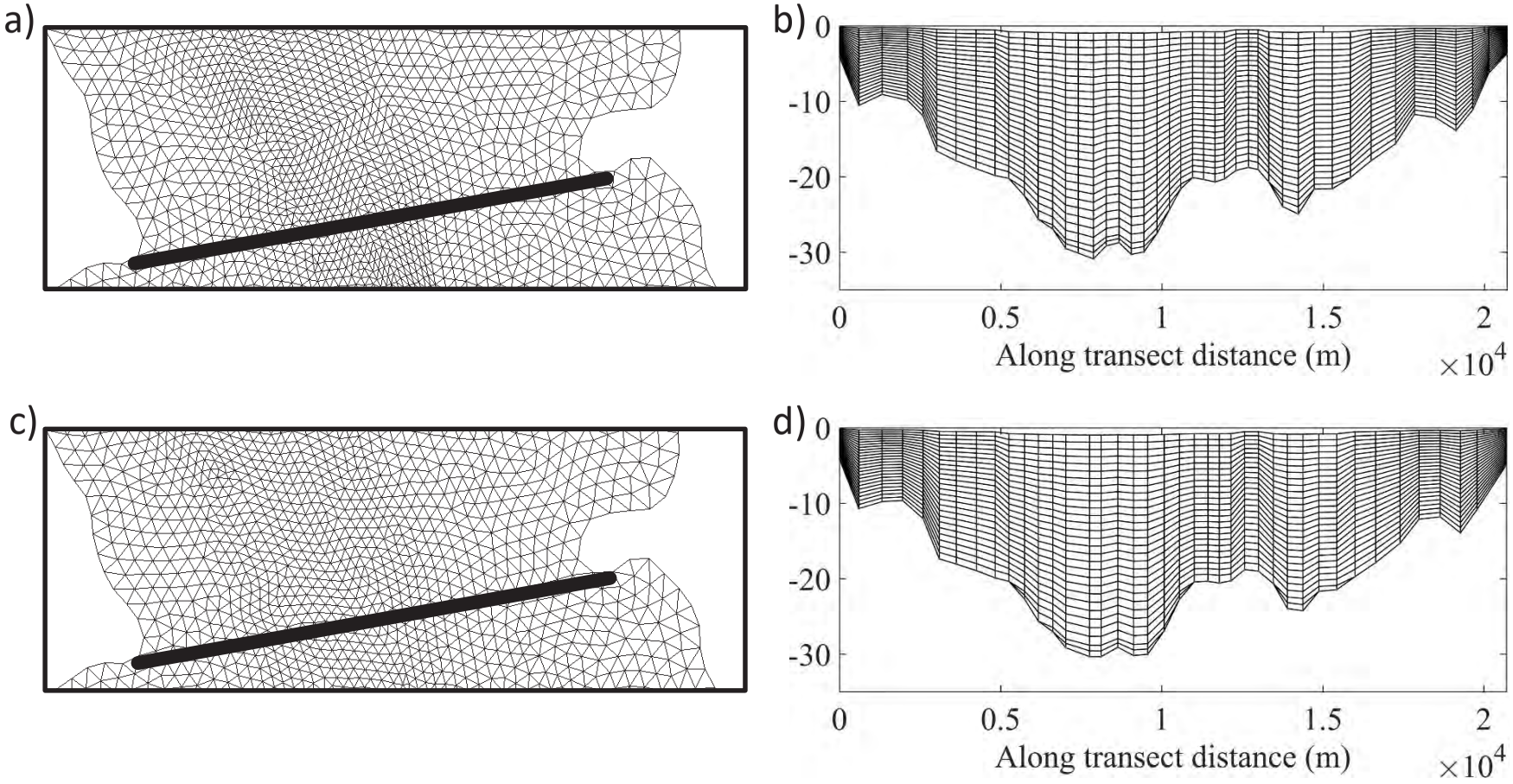
a)
b)
0
-10
-20
-30
0
0.5
1
1.5
2
Along transect distance (m)
×10^4
c)
d)
0
-10
-20
-30
0
0.5
1
1.5
2
Along transect distance (m)
×10^4

Fig. S2.

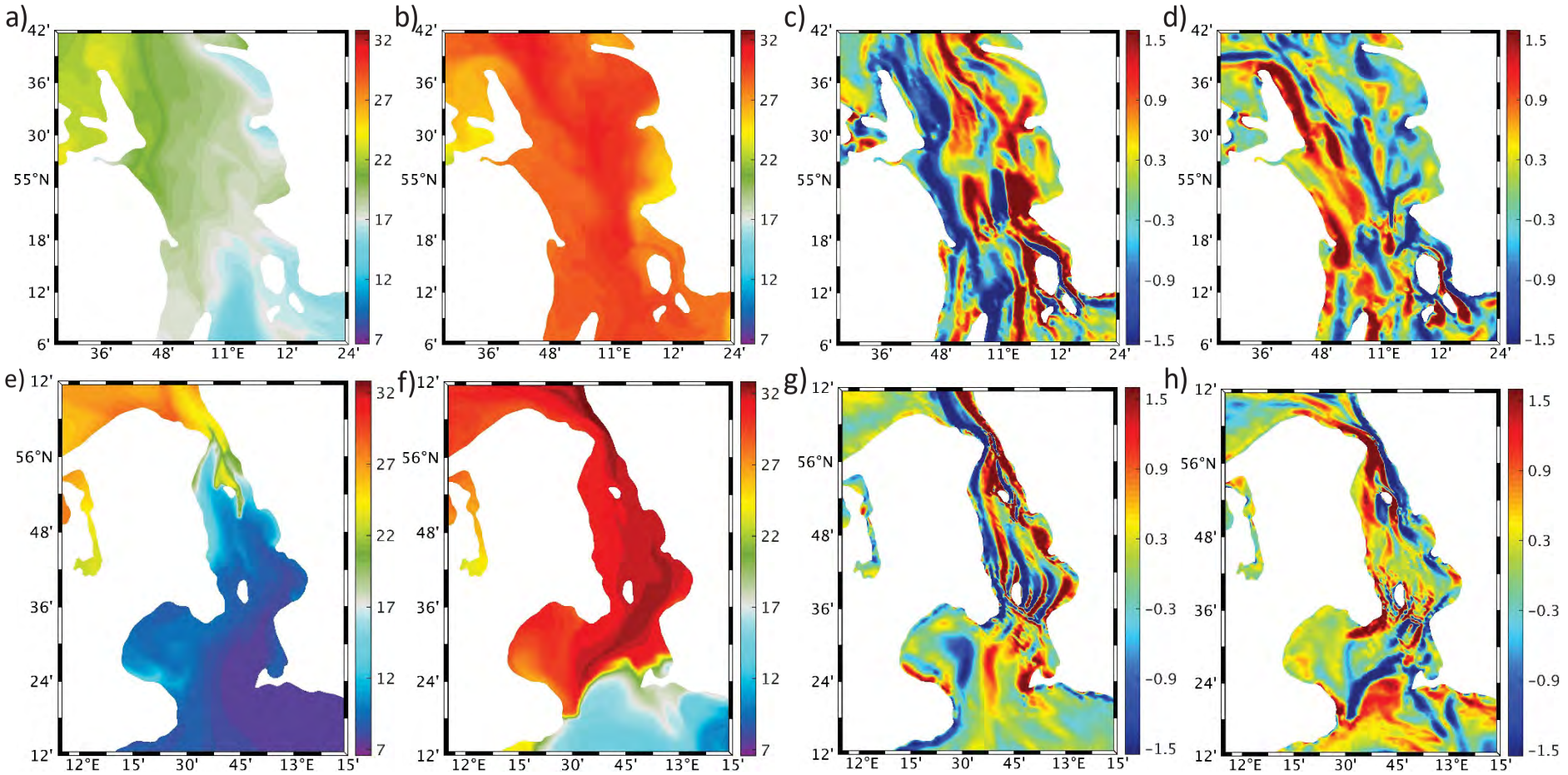
a)
b)
c)
d)
e)
f)
g)
h)
42'
36'
30'
55°N
18'
12'
6'
36'
48'
11°E
12'
24'
32
27
22
17
12
7
1.5
0.9
0.3
-0.3
-0.9
-1.5
12'
56°N
48'
36'
24'
12°E
15'
30'
45'
13°E

Fig. S3.

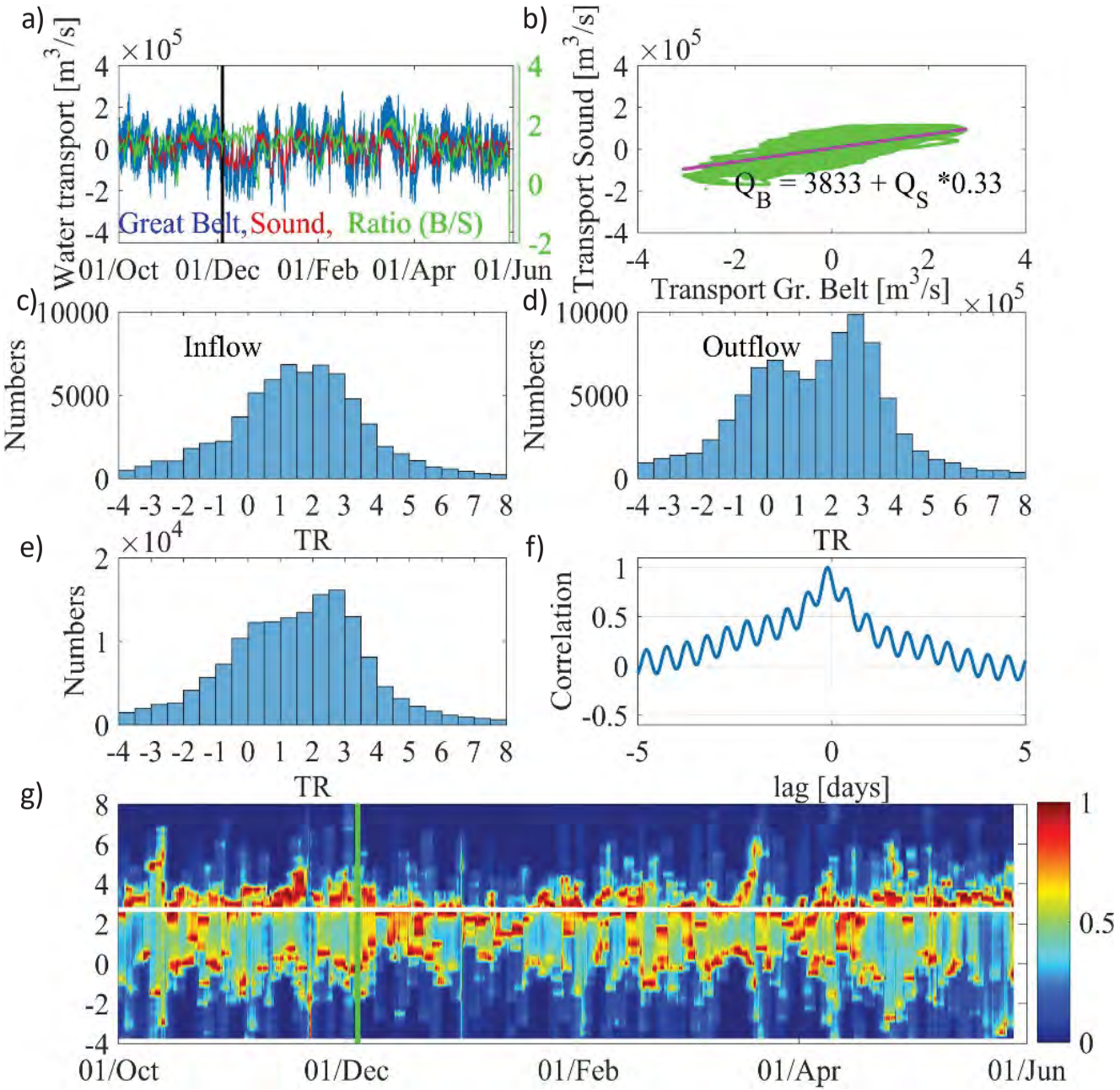
a)
Water transport [m3/s]
×10^5
Great Belt, Sound, Ratio (B/S)
01/Oct 01/Dec 01/Feb 01/Apr 01/Jun
b)
Transport Sound [m3/s]
Transport Gr. Belt [m3/s]
×10^5
QB = 3833 + QS *0.33
c)
Numbers
Inflow
d)
Outflow
×10^5
e)
×10^4
TR
f)
Correlation
lag [days]
g)
01/Oct
01/Dec
01/Feb
01/Apr
01/Jun

Fig. S4.

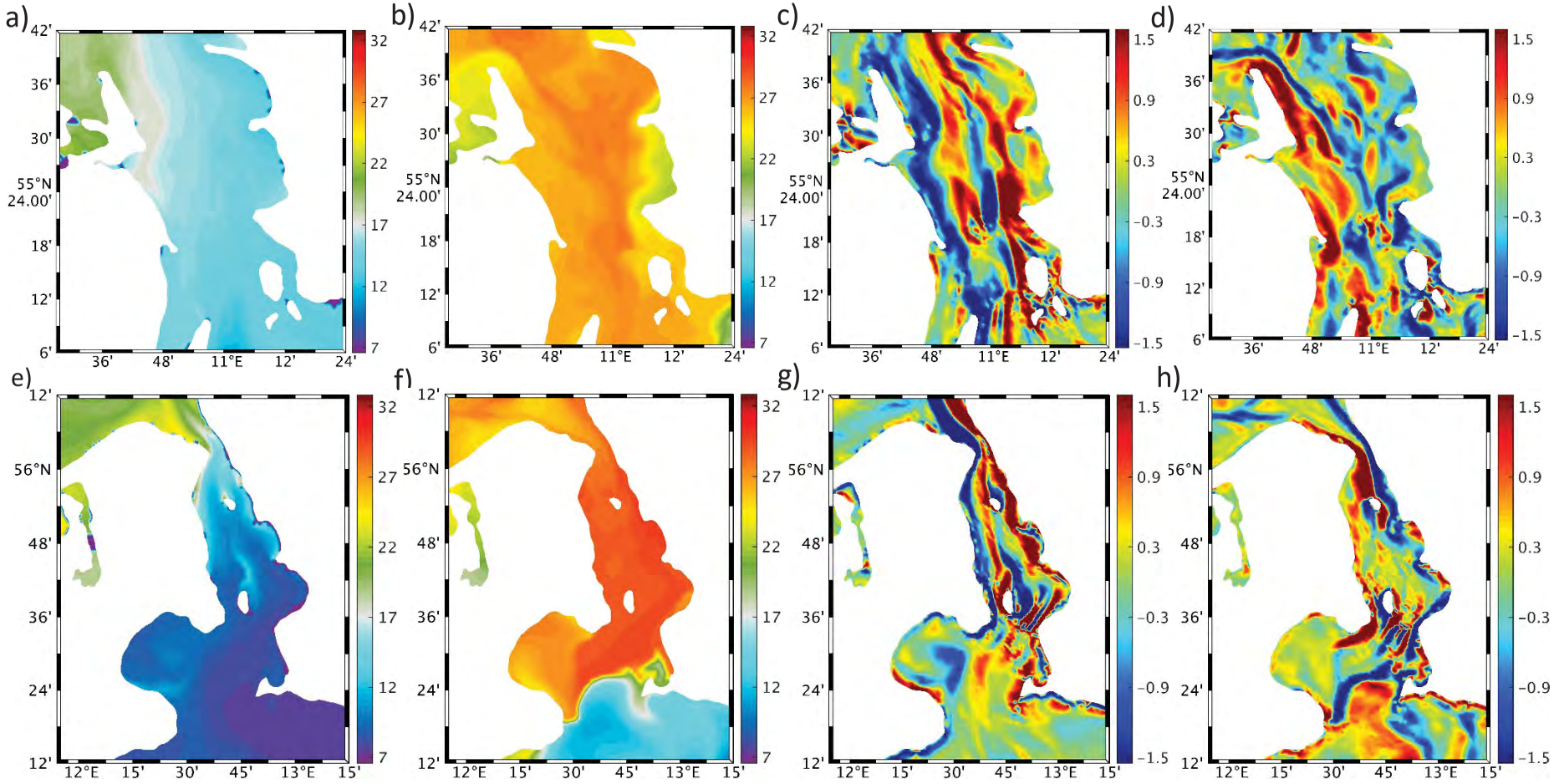
a)
b)
c)
d)
e)
f)
g)
h)
42'
36'
30'
55°N
24.00'
18'
12'
6'
36'
48'
11°E
12'
24'
32
27
22
17
12
7
1.5
0.9
0.3
-0.3
-0.9
-1.5
12'
48'
36'
24'
56°N
12°E
15'
30'
45'
13°E

Fig. S5.